



Antibacterial activity of xylose-derived LpxC inhibitors – Synthesis, biological evaluation and molecular docking studies

Alexander Dreger^{a,b}, Katharina Hoff^{a,b}, Oriana Agoglitta^{a,b}, Sven-Kevin Hotop^c, Mark Brönstrup^{c,d}, Peter Heisig^e, Johannes Kirchmair^{f,g}, Ralph Holl^{a,b,*}

^a Institute of Organic Chemistry, University of Hamburg, Martin-Luther-King-Platz 6, 20146 Hamburg, Germany

^b German Center for Infection Research (DZIF), Partner Site Hamburg-Lübeck-Borstel-Riems, Germany

^c Department of Chemical Biology, Helmholtz Centre for Infection Research (HZI), Inhoffenstr. 7, 38124 Braunschweig, Germany

^d German Center for Infection Research (DZIF), Partner Site Hannover-Braunschweig, Germany

^e Institute of Biochemistry and Molecular Biology, University of Hamburg, Bundesstr. 45, 20146 Hamburg, Germany

^f Department of Pharmaceutical Chemistry, University of Vienna, Althanstrasse 14, 1090 Vienna, Austria

^g Center for Bioinformatics (ZBH), University of Hamburg, Bundesstr. 43, 20146 Hamburg, Germany

ARTICLE INFO

Keywords:

Antibiotics
LpxC inhibitors
C-glycosides
Molecular docking studies
Bacterial uptake

ABSTRACT

LpxC inhibitors represent a promising class of novel antibiotics selectively combating Gram-negative bacteria. In chiral pool syntheses starting from D- and L-xylose, a series of four 2*r*,3*c*,4*t*-configured C-furanosidic LpxC inhibitors was obtained. The synthesized hydroxamic acids were tested for antibacterial and LpxC inhibitory activity, the acquired biological data were compared with those of previously synthesized C-furanosides, and molecular docking studies were performed to rationalize the observed structure-activity relationships. Additionally, bacterial uptake and susceptibility to efflux pump systems were investigated for the most promising stereoisomers.

1. Introduction

The excessive and broad use of antibiotics in human medicine and livestock breeding has exposed bacteria to high selection pressure, which has led to the establishment and extension of mechanisms of resistance against the employed antibiotics, resulting in multidrug- and even pandrug-resistant bacteria [1,2]. Especially multidrug-resistant Gram-negative bacteria, such as *Escherichia coli* and *Pseudomonas aeruginosa*, pose a serious threat to human health and welfare, being mainly responsible for severe and often lethal nosocomial infections [3–7]. As even last-resort antibiotics have been reported to be ineffective against numerous bacterial strains, there is an urgent need for the development of novel antibacterial drugs, ideally addressing so far unexploited bacterial targets [8–12].

One such target is the bacterial deacetylase LpxC, which is indispensable for the biosynthesis of lipid A, the hydrophobic membrane anchor of the lipopolysaccharides (LPS). Lipid A essentially contributes to the integrity of the outer membrane of Gram-negative bacteria and thus to their viability and virulence [13–16]. Consequently, the inhibition of LpxC is lethal to Gram-negative bacteria [17], which, together

with the fact that the enzyme shows no sequence homology to any mammalian enzyme but is highly conserved among Gram-negative bacteria, makes the deacetylase a very promising target for antibacterial drug development.

The Zn²⁺-dependent enzyme LpxC catalyzes the second and committed step in the biosynthesis of lipid A, which in *E. coli* is the irreversible deacetylation of UDP-3-*O*-[(*R*)-3-hydroxymyristoyl]-*N*-acetylglucosamine (1, Fig. 1a) [18,19]. The enzyme displays a “β-α-β sandwich fold”, being formed by two domains with similar topologies. At one side of the sandwich, the conical active site cleft of the enzyme is located. At its bottom, the catalytic Zn²⁺-ion is complexed by one aspartate and two histidine residues (i.e. Asp242, His79, and His238 in case of *E. coli* LpxC). A crystal structure of the deacetylated product 2 in complex with *E. coli* LpxC gave insight into substrate recognition by the enzyme (Fig. 1b) [20]. Whereas the glucosamine moiety binds upon a hydrophobic patch formed by Phe192 and Phe194, it additionally interacts with the enzyme via a water-mediated contact to Asp242 and a direct interaction between the 6'-OH group and Lys239, which also recognizes the phosphate groups. A hydrophobic tunnel, composed of residues Met195, Ile198, Phe212 and Val217, leads out of the active site

* Corresponding author at: Institute of Organic Chemistry, University of Hamburg, Martin-Luther-King-Platz 6, 20146 Hamburg, Germany.

E-mail address: ralph.holl@chemie.uni-hamburg.de (R. Holl).

cleft, binding the fatty acyl chain of the enzyme's natural substrate **1** during catalysis. The latter has been proposed to proceed via a general acid/base mechanism, with Glu78 and His265 acting as general base and general acid, respectively, and Thr191 stabilizing the intermediately formed tetrahedral *gem*-diolate [20,21].

Various LpxC inhibitors have already been described in the literature [22,23]. As common structural features, most of these inhibitors exhibit a Zn^{2+} -chelating hydroxamate moiety and a long hydrophobic substituent addressing the hydrophobic tunnel of the enzyme. Thus, for example, the *N*-aroyl-L-threonine hydroxamic acids CHIR-090 (**3**) and LPC-011 (**4**) (Fig. 2) represent potent LpxC inhibitors [24–26]. A crystal structure of *E. coli* LpxC in complex with LPC-011 (**4**) shows that the threonyl-hydroxamate head group of the inhibitor occupies the active site, undergoing interactions with conserved residues like Glu78, Thr191, Phe192, Lys239, and His265, whereas the diphenyldiacetylene moiety of the inhibitor penetrates through the enzyme's hydrophobic tunnel [24].

As the natural substrate **1** of LpxC is an amino sugar derivative, additionally, carbohydrate-based inhibitors were developed. Thus, one of the first reported LpxC inhibitors was the substrate analog TU-514 (**5**). TU-514 (**5**) inhibits a broad range of LpxC orthologues but was found not to exhibit any antibacterial activity [27–29].

Recently, we reported on the synthesis and biological evaluation of a series of C-furanosidic LpxC inhibitors [30–37]. These conformationally constrained compounds bear the Zn^{2+} -chelating hydroxamate moiety and the lipophilic side chain in positions 2 and 5 of their tetrahydrofuran ring, respectively, whereas two hydroxy groups are found in positions 3

and 4. We have started to vary the stereochemistry of these compounds and have already accomplished the synthesis of all eight 3,4-*cis*-configured stereoisomers (**6–9**, *ent*-**6**–*ent*-**9**). Among these compounds, the (2*S*,3*S*,4*R*,5*S*)-configured dihydroxytetrahydrofuran derivative **8** was found to exhibit the highest inhibitory and antibacterial activity (Table 1). To gain further insight into the relationship between the stereochemistry of these C-furanosidic compounds and their biological activity, the so far unexplored 3,4-*trans*-configured stereoisomers would need to be tested. Therefore, in this paper, we wish to report on the synthesis and biological evaluation of a series of 3,4-*trans*-configured dihydroxytetrahydrofuran derivatives that are derived from D- and L-xylose. Thus, based on the stereochemistry of these enantiomeric sugars, all of the newly synthesized C-furanosidic LpxC inhibitors (**10**, **11**, *ent*-**10**, *ent*-**11**) exhibit 2*r*,3*c*,4*t*-configuration, bearing the hydroxamate moiety and the adjacent 3-hydroxy group on the same side of the tetrahydrofuran ring. Additionally, a more in-depth biological evaluation of the most potent stereoisomers is presented.

2. Results and discussion

2.1. Chemistry

The series of 3,4-*trans*-configured dihydroxytetrahydrofuran derivatives was obtained in chiral pool syntheses starting from D- and L-xylose. First, in a two-step one-pot procedure, comprising an initial anomeric oxidation with bromine and a subsequent acetalization with benzaldehyde, D-xylose (**12**) was transformed into benzylidene-

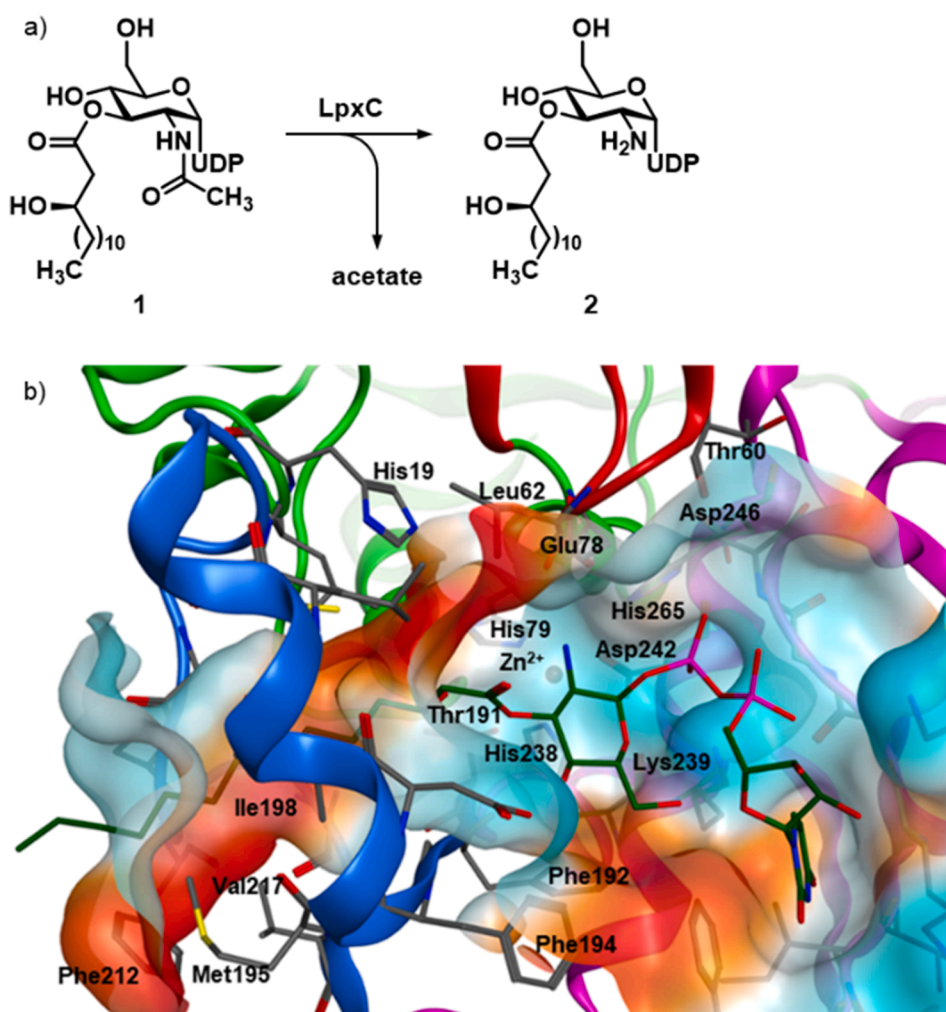


Fig. 1. a) LpxC-catalyzed deacetylation of UDP-3-O-[(R)-3-hydroxymyristoyl]-N-acetylglucosamine (**1**). b) Molecular surface of *E. coli* LpxC near the deacetylated natural product **2** (PDB 4MDT) [20]. **2** is shown as dark green stick model. Amino acid residues in proximity to the surface are depicted as gray stick models. Oxygen, nitrogen, sulfur, and phosphorus atoms are colored in red, blue, yellow, and magenta, respectively. The Zn^{2+} -ion is depicted as gray sphere. The surface is colored as follows: lipophilic regions are in orange, hydrophilic in cyan, and neutral in white [22] (For interpretation of the references to colour in this figure legend, the reader is referred to the web version of this article.)

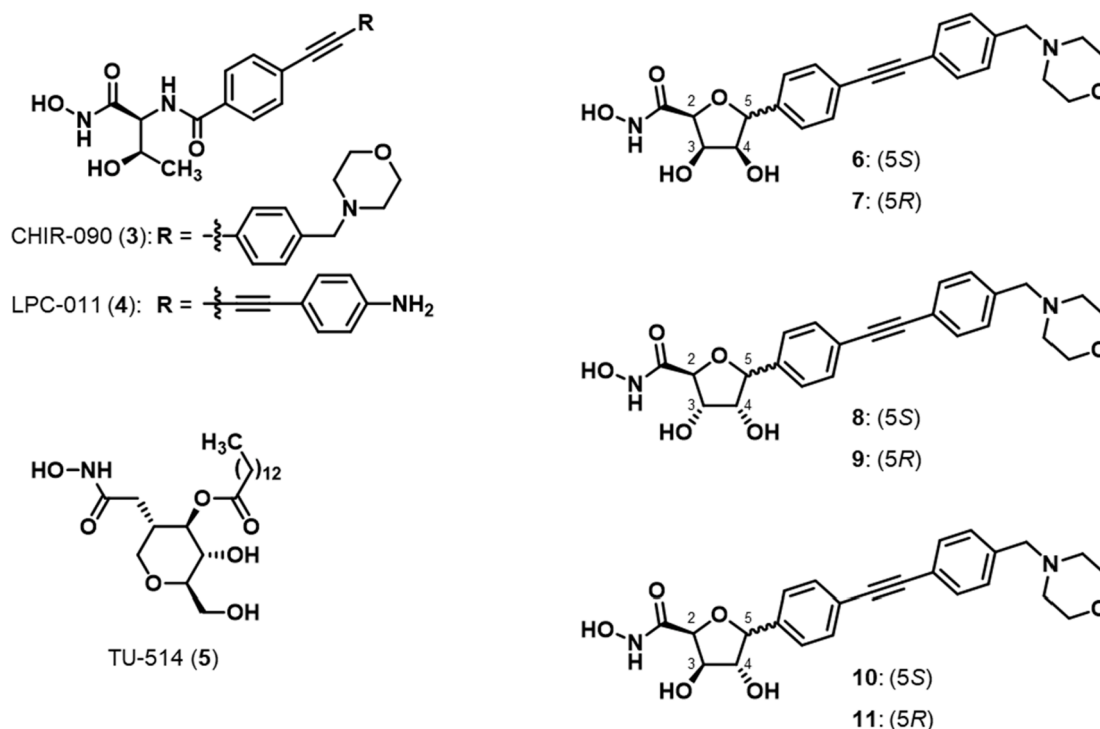


Fig. 2. Structures of described and envisaged LpxC inhibitors.

protected lactone **13** (Scheme 1) [38–40]. After MOM-protection of the remaining hydroxy group of **13**, the thereby obtained fully protected lactone **14** was reacted with 4-iodophenyllithium, which could be generated *in situ* from 1,4-diodobenzene and *n*-butyllithium, to yield hemiketal **15** [30,36–37]. To afford the desired *C*-glycosidic scaffold, hemiketal **15** was subjected to a reduction with triethylsilane in the presence of boron trifluoride diethyl etherate in acetonitrile at $-40\text{ }^{\circ}\text{C}$ [41]. However, under these conditions, the acetal moieties were partially cleaved. As the resulting diastereomeric *C*-furanosides could be separated best *via* flash column chromatography in their benzylidene-protected form, the crude product of the reduction was reacted with benzaldehyde and conc. H_2SO_4 to yield the benzylidene-protected anomeric *C*-aryl furanosides **16** and **17**. After their separation, the benzylidene moieties of *C*-furanosides **16** and **17** were cleaved under acidic conditions, yielding triols **18** and **19**, respectively. Subsequently, the 2-hydroxymethyl groups of tetrahydrofuran derivatives **18** and **19** were transformed into ester moieties *via* a selective oxidation followed by a *p*-toluenesulfonic acid-catalyzed esterification of the intermediate carboxylic acids with methanol to give methyl esters **20** and **21**. Whereas the (5*S*)-configured tetrahydrofuran derivative **18** was oxidized with TEMPO and *N*-chlorosuccinimide in one step, the oxidation of its (5*R*)-configured diastereomer **19** was performed in two steps, comprising an initial reaction with Dess-Martin periodinane followed by a silver nitrate-mediated oxidation of the intermediately formed aldehyde [42–45]. The configuration at the anomeric center of the synthesized *C*-glycosides could be unequivocally proven by an X-ray crystal structure of ester **20** (Fig. S1). The obtained crystal structure shows that the tetrahydrofuran ring adopts an envelope conformation, with the C11 atom lying most distinctive out of the mean plane by 0.2631(19) Å. The puckering parameters calculated with PLATON according to Cremer & Pople [46] are $Q = 0.4164(19)\text{ \AA}$ and $\Phi = 69.5(2)^{\circ}$ for the tetrahydrofuran ring O14/C10/C11/C12/C13. The absolute configurations at atoms C10, C11, C12, and C13 of the five membered ring are *S*, *R*, *R*, and *S*, respectively.

To build up the lipophilic side chain of the envisaged LpxC inhibitors, aryl iodides **20** and **21** were subjected to Sonogashira couplings with 4-(morpholinomethyl)phenylacetylene to yield diphenylacetylene

derivatives **22** and **23**, respectively [30]. Subsequent aminolyses of esters **22** and **23** with hydroxylamine finally gave the desired hydroxamic acids **10** and **11**.

The corresponding enantiomers *ent*-**10** and *ent*-**11** were obtained in principally the same way, starting from L-xylose.

2.2. Biological evaluation

In order to evaluate the antibacterial activity of the xylose-derived *C*-furanosides against *E. coli* BL21(DE3) and *E. coli* D22, disc diffusion assays were carried out and their minimum inhibitory concentrations (MIC) were determined. Due to a *lpxC* gene mutation, the *E. coli* D22 strain exhibits only about 5% of wild-type LpxC activity, leading to a defective formation of the cell envelope [47–49]. Thus, the cell envelope of *E. coli* D22 cells is more permeable for antibacterial compounds and already a modest LpxC inhibition has a strong impact on the viability of these bacteria.

The compounds' inhibitory activity was determined in a fluorescence-based enzyme assay using the *E. coli* LpxCC63A enzyme [17]. The C63A mutation lowers the undesired susceptibility of the wild-type enzyme to inhibition by high Zn^{2+} concentrations [50,51].

All of the newly synthesized compounds were found to exhibit inhibitory activity toward LpxC. They all showed antibacterial activity against *E. coli* D22 ($\text{MIC} \leq 64\text{ }\mu\text{g}\cdot\text{mL}^{-1}$) and, except for *ent*-**10**, a moderate activity against *E. coli* BL21(DE3) as shown by the agar diffusion test. With respect to inhibitory ($K_i = 5.3\text{ }\mu\text{M}$) as well as antibacterial activity (MIC against *E. coli* D22 = $8\text{ }\mu\text{g}\cdot\text{mL}^{-1}$, highest zone diameter for both strains), the (2*S*,3*R*,4*R*,5*S*)-configured compound **10** was found to be the most potent compound of this series of xylose-derived *C*-furanosides.

2.3. Molecular docking studies

In order to rationalize the experimentally observed biological activities of the stereoisomeric *C*-furanosides, all 12 stereoisomers were docked into a crystal structure of *Ec*LpxC (PDB ID: 3PS3) [24]. The docking poses of the *C*-furanosides show that the narrow, hydrophobic

Table 1
Antibacterial and LpxC inhibitory activities of the investigated hydroxamic acids.

Compound	zone of inhibition [mm]	MIC [$\mu\text{g}\cdot\text{mL}^{-1}$]		IC ₅₀ [μM]	K _i [μM]		
		<i>E. coli</i> BL21(DE3)	<i>E. coli</i> D22			<i>E. coli</i> BL21(DE3)	<i>E. coli</i> D22
6	(2 <i>S</i> ,3 <i>R</i> ,4 <i>S</i> ,5 <i>S</i>)	≤6	13.4 ± 1.8	>64	8	>200	>27.6
<i>ent</i> -6	(2 <i>R</i> ,3 <i>S</i> ,4 <i>R</i> ,5 <i>R</i>)	≤6	≤6	>64	>64	>200	>27.6
10	(2 <i>S</i> ,3 <i>R</i> ,4 <i>R</i> ,5 <i>S</i>)	15.0 ± 1.4	22.3 ± 2.1	>64	8	38.6 ± 19.4	5.3 ± 2.7
<i>ent</i> -10	(2 <i>R</i> ,3 <i>S</i> ,4 <i>S</i> ,5 <i>R</i>)	≤6	10.5 ± 1.2	>64	64	151.0 ± 36.6	20.8 ± 5.1
8	(2 <i>S</i> ,3 <i>S</i> ,4 <i>R</i> ,5 <i>S</i>)	22.3 ± 1.4	28.3 ± 1.4	8	0.5	3.2 ± 1.0	0.4 ± 0.1
<i>ent</i> -8	(2 <i>R</i> ,3 <i>R</i> ,4 <i>S</i> ,5 <i>R</i>)	15.1 ± 1.5	25.7 ± 2.0	>64	2	28.2 ± 9.0	3.9 ± 1.2
7	(2 <i>S</i> ,3 <i>R</i> ,4 <i>S</i> ,5 <i>R</i>)	9.7 ± 0.5	21.4 ± 2.3	>64	8	34 ± 10	4.7 ± 1.4
<i>ent</i> -7	(2 <i>R</i> ,3 <i>S</i> ,4 <i>R</i> ,5 <i>S</i>)	11.0 ± 0.8	19.7 ± 1.3	>64	64	90 ± 35.6	12.4 ± 4.9
11	(2 <i>S</i> ,3 <i>R</i> ,4 <i>R</i> ,5 <i>R</i>)	11.0 ± 2.3	17.5 ± 3.0	>64	32	149.1 ± 30.7	20.6 ± 4.2
<i>ent</i> -11	(2 <i>R</i> ,3 <i>S</i> ,4 <i>S</i> ,5 <i>S</i>)	10.0 ± 1.7	18.8 ± 2.1	>64	32	185.6 ± 51.5	25.6 ± 7.0
9	(2 <i>S</i> ,3 <i>S</i> ,4 <i>R</i> ,5 <i>R</i>)	14.0 ± 1.0	21.0 ± 0.5	>64	32	127.4 ± 15.6	17.6 ± 2.2
<i>ent</i> -9	(2 <i>R</i> ,3 <i>R</i> ,4 <i>S</i> ,5 <i>S</i>)	6.8 ± 1.0	22.8 ± 2.2	>64	4	10 ± 1.0	1.4 ± 0.2

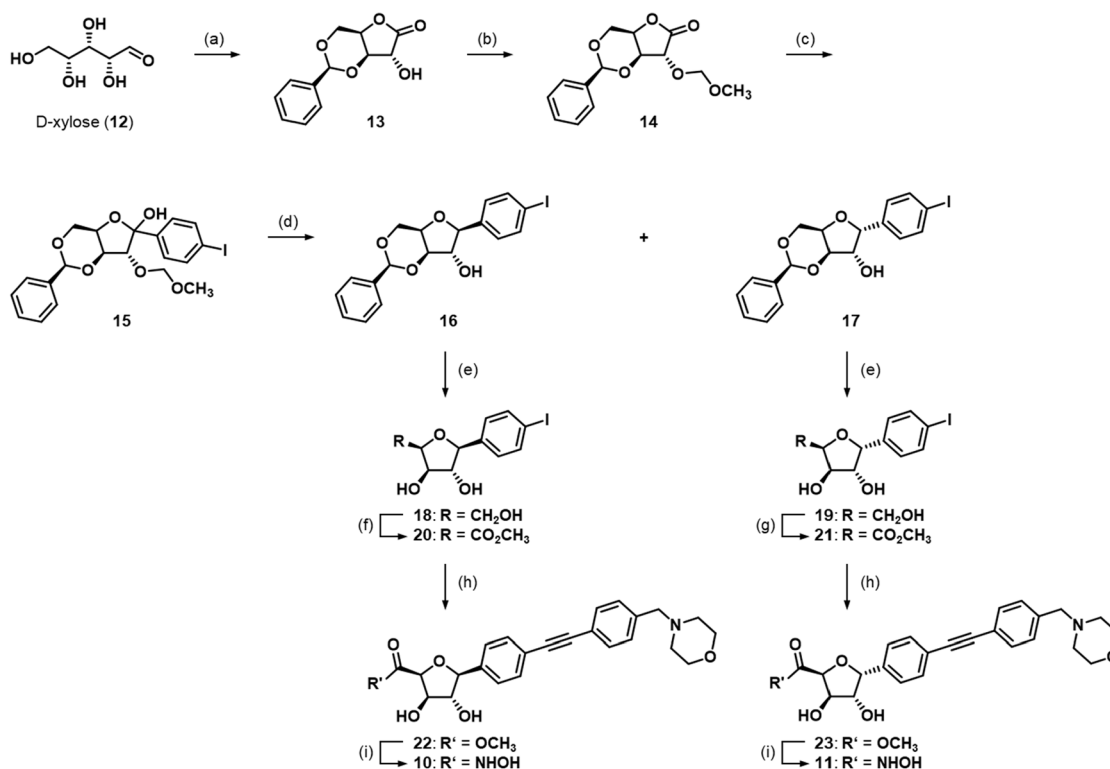
tunnel leading to the active site of LpxC is filled by the diphenylacetylene moiety common to all investigated synthetic inhibitors (Fig. 3). The deep and largely hydrophilic part of the ligand binding pocket is occupied by the hydroxamic acid moiety, chelating the catalytic Zn²⁺-ion, and the furanose moiety, acting as linker and important mediator of protein-ligand interactions.

Earlier docking studies with the 3,4-*cis*-configured *C*-furanosides suggested already that highly active compounds such as **8** may form a tight hydrogen bond network with several amino acids in its vicinity, including Met61 (amide oxygen), Cys63 (amide nitrogen and oxygen), Thr191 (hydroxyl moiety), Phe192 (amide oxygen), and His265 (Ne²) [37]. Importantly, many of the interactions predicted to be formed between the ligand and the protein backbone are mediated by the water molecules W1053 and W1058.

Docking experiments with all 12 *C*-furanosides discussed in this work indicate that the (2*S*,3*S*,4*R*,5*S*)-configuration of **8** enables the compound to adopt the most suitable conformation for ligand binding, both with

respect to protein-ligand shape complementarity and the formation of a tight network of (in part water-mediated) hydrogen bond interactions (Fig. 3A; Table 2). This is consistent with the fact that the lowest IC₅₀ was measured for this compound. *ent*-**9**, the compound with the second lowest IC₅₀ value, is predicted to induce a minor dislocation of W1058 in order to maintain parts of the water-mediated network of hydrogen bonds interactions (Fig. 3B; dislocated W1058 not shown). *ent*-**8**, the compound with the third lowest IC₅₀ value is predicted to displace the conserved W1058 in order to fit to the binding pocket (Fig. 3C). It is therefore likely that this compound lacks interactions with Thr60 and Cys63. The docking poses obtained for any of the compounds with lower IC₅₀ values, such as the one for **10** (Fig. 3D) suggest the absence of key interactions including, in some cases, the lack of a chelation of the Zn²⁺-ion (Table 2).

Whereas a clear relationship between the quality of the predicted hydrogen bond network and the measured IC₅₀ values was observed (Table 2), no correlation between the docking scores (not shown) and



Scheme 1. Reagents and conditions: (a) 1. Br_2 , K_2CO_3 , H_2O , $0^\circ\text{C} \rightarrow \text{rt}$, 2. benzaldehyde, conc. H_2SO_4 , rt, 33%; (b) NaH, $\text{ClCH}_2\text{OCH}_3$, THF, $-20^\circ\text{C} \rightarrow \text{rt}$, 73%; (c) 1,4-diiodobenzene, *n*-BuLi, THF, -78°C , then **14**, 50%; (d) 1. Et_3SiH , $\text{BF}_3\cdot\text{OEt}_2$, ACN, -40°C , 2. benzaldehyde, conc. H_2SO_4 , THF, rt, **16** 33%, **17** 23%; (e) conc. HCl, ACN, rt, **18** 45%, **19** 50%; (f) 1. DMP, ACN, rt, 2. AgNO_3 , KOH, $\text{H}_2\text{O}/\text{ACN}$, rt, 3. *p*-TsOH, MeOH, Δ , 44%; (g) 1. TEMPO, NCS, ACN/aq. NaHCO_3 (1/1), 50°C , 2. *p*-TsOH, MeOH, Δ , 53%; (h) 4-(morpholinomethyl)phenylacetylene, $\text{Pd}(\text{PPh}_3)_4$, CuI, NEt_3 , ACN, rt, **22** 48%, **23** 68%; (i) $\text{NH}_2\text{OH}\cdot\text{HCl}$, NaOMe, MeOH, rt, **10** 52%, **11** 18%.

the measured bioactivities was found, which is again consistent with previous findings [37].

2.4. Structure-activity relationships

In earlier work by some of us [37], it was observed that the inversion of configuration in positions 3 and 4 of the inactive, all-*cis*-configured *C*-furanosides **6** and *ent*-**6**, leading to compounds **8** and *ent*-**8**, causes a pronounced increase in antibacterial and inhibitory activity. In the current study, it was found that the sole inversion of the stereocenter in position 4, leading to the newly synthesized compounds **10** and *ent*-**10**, has an intermediate effect. Thus, compounds **10** and *ent*-**10** are considerably more active than the respective all-*cis*-configured epimer, but less active than the respective 2,3-*trans*-configured epimer, each.

The reduced inhibitory activity of **10** compared to **8** can be rationalized from the docking poses of the two compounds. The inversion of configuration in position 3 in the case of **10** is expected to lead to a loss of the water-mediated hydrogen bond with Phe192, caused by the displacement of W1053. Even though the furanose moiety of **10** may form an additional hydrogen bond with Thr191, this interaction is likely unable to compensate for the loss of the hydrogen bonds mediated by W1053.

Previously it has been shown that also the inversion of either the stereocenter in position 2 or the stereocenter in position 5 of **6** and *ent*-**6** leads to an increase in inhibitory and antibacterial activity: *ent*-**9** and **7** were more active than **6**, and **9** and *ent*-**7** obtained higher activity than *ent*-**6**, respectively. However, the trend that switching a single stereocenter of **6** and *ent*-**6** yields more active compounds is least pronounced in the case of the inversion of configuration in position 4, especially with respect to inhibitory activity toward LpxC. When comparing the respective pairs of enantiomers, it can be observed that the compounds resulting from the inversion of one sole stereocenter of **6** (i.e. **10**, *ent*-**9**,

and **7**) represent the more active enantiomer, each.

As stated before, starting from the least active, all-*cis*-configured *C*-furanosides **6** and *ent*-**6**, the inversion of configuration of the two stereocenters in positions 3 and 4 led to a strong increase in inhibitory activity. The simultaneous inversion of the two stereocenters in positions 2 and 3, leading to compounds **11** and *ent*-**11**, also increased inhibitory activity. However, the two compounds do not outperform the doubly inverted, 3,4-*cis*-configured stereoisomers **8** and *ent*-**8**. Docking suggests that the configuration of *C*-furanoside **11** forces the ligand to adopt a conformation that is less favorable for the formation of interactions with the catalytic Zn^{2+} -ion and the surrounding hydrogen bonding partners (the automated docking protocol did not produce any poses with the hydroxamic acid moiety oriented towards the Zn^{2+} -ion).

When comparing compounds **11** and *ent*-**11** with the other 2,5-*trans*-configured *C*-furanosides (**7**, *ent*-**7**, **9**, and *ent*-**9**), the two newly synthesized compounds were found to be the least potent LpxC inhibitors of this subset of stereoisomers.

The further comparison of the relative configuration of the stereocenters shows that placing the hydroxamate moiety and the neighboring hydroxy group on opposite sides of the tetrahydrofuran ring seems to be beneficial for the biological activity of the compounds. The same applies to the lipophilic side chain and its adjacent hydroxy group. Thus, compounds **8** and *ent*-**8**, exhibiting 2,3-*trans*- and 4,5-*trans*-configuration, represent the most active stereoisomers of the investigated series of *C*-furanosides.

A comparison of the stereochemistry of compounds **8**, *ent*-**9**, *ent*-**8**, **7**, and **10**, the most potent LpxC inhibitors ($\text{IC}_{50} < 40 \mu\text{M}$) of the presented series of *C*-furanosides, shows that among these compounds all four stereocenters can be found in both configurations. Apparently, there is not one single stereocenter, which is obligatorily required to exhibit a certain configuration for high inhibitory activity. It is rather the interplay of the stereocenters, which needs to be considered, as all of the

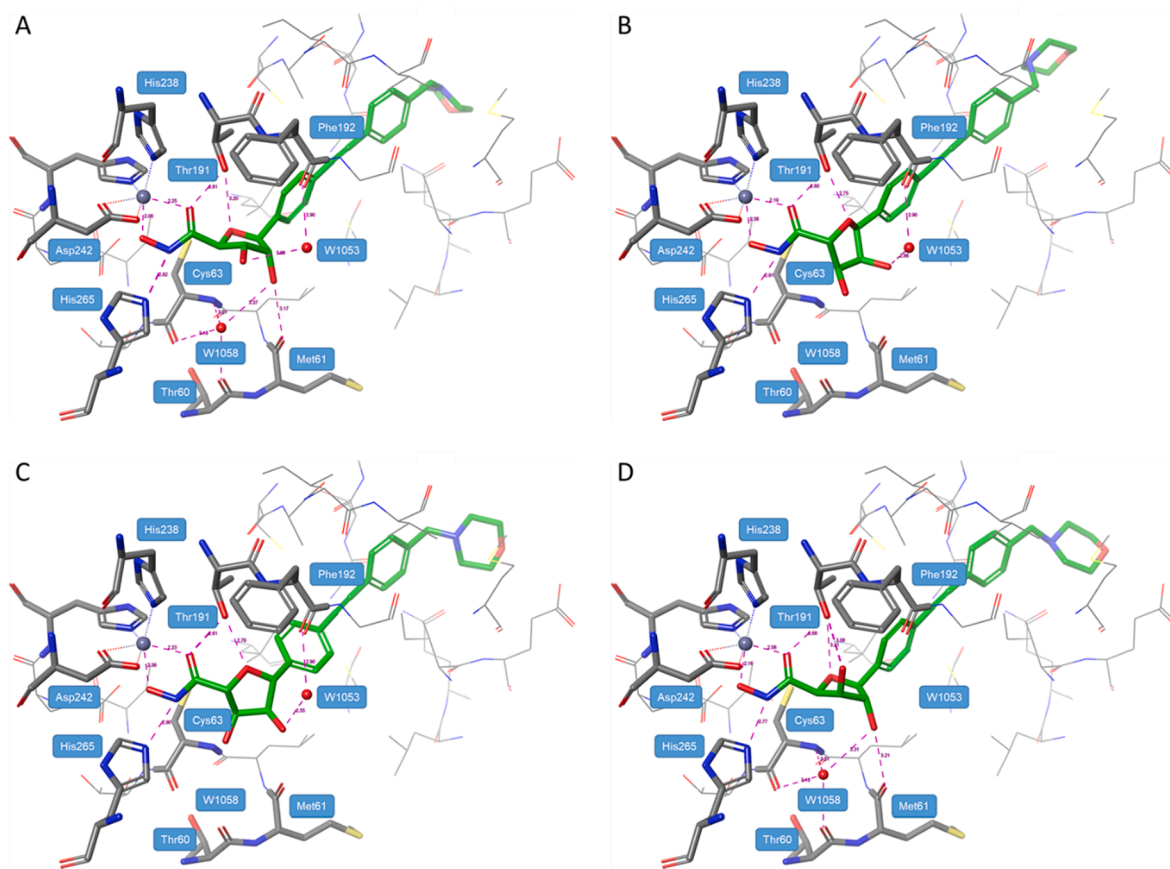


Fig. 3. Predicted binding modes of (A) **8**, (B) *ent-9*, (C) *ent-8* and (D) **10**. The compounds and the most relevant amino acids are highlighted in sticks mode. The Zn^{2+} -ion and water molecules are represented as purple and red spheres, respectively. Metal and hydrogen bond interactions are indicated by the purple, dashed lines. (For interpretation of the references to colour in this figure legend, the reader is referred to the web version of this article.)

Table 2
Predicted interactions formed between the investigated hydroxamic acids and LpxC.

Activity rank ^a	Compound	Chelation with Zn^{2+}	H-bond with						
			Thr60 ^b and Cys63 ^b	Met61 ^b	Thr191 ^c	Phe192 ^b	His265	W1053	W1058
1	8	+	+ (via W1058)	+	++	++ (via W1053)	+	+	+
2	<i>ent-9</i>	+	+/-	+/-	++	+ (via W1053)	+	+	minor dislocation by ligand expected
3	<i>ent-8</i>	+	-	+/-	++	+ (via W1053)	+	+	displacement by ligand expected
4	7	no pose interacting with Zn^{2+} was obtained ^d							
5	10	+	++ (via W1058)	+	++	-	+	-	+
6	<i>ent-7</i>	no pose interacting with Zn^{2+} was obtained ^d							
7	9	no pose interacting with Zn^{2+} was obtained ^d							
8	11	no pose interacting with Zn^{2+} was obtained ^d							
9	<i>ent-10</i>	no pose interacting with Zn^{2+} was obtained ^d							
10	<i>ent-11</i>	+	-	-	++	-	+	minor dislocation by ligand expected	displacement by ligand expected
11	6	+	-	-	++	+	+	minor dislocation by ligand expected	-
12	<i>ent-6</i>	no pose interacting with Zn^{2+} was obtained ^d							

^a Activity rank according to IC_{50} measured for LpxC from *EcLpxCC63A*.

^b Interaction with the protein backbone (amide oxygen).

^c Interaction with the amino acid side chain (hydroxy group).

^d In both the presence and absence of solvent molecules.

highly active compounds - despite their diverging stereochemistry - are able to form direct hydrogen bonds with Met61 and Thr191.

2.5. Cellular uptake and efflux

The presence of efflux pump systems, actively transporting a large variety of toxic compounds from the bacterial cytoplasm to the outside environment, is an important contributor to the intrinsic resistance of Gram-negative bacteria to many antibacterial compounds. Additionally, bacteria can acquire resistance by further decreasing membrane permeability. Thus, down-regulation of outer membrane porins (OMPs), the protein channels through which hydrophilic compounds enter the bacterial cell, and up-regulation of efflux pumps are mechanisms of resistance that have been reported alone and in combination in a number of multidrug-resistant isolates [52,53].

Therefore, we investigated whether the synthesized *C*-glycosides are able to penetrate the bacterial cell wall and reach their cytoplasmic target, and whether they are substrates of multidrug resistance (MDR) efflux pump systems. Thus, **8** and *ent*-**8**, being the two most potent LpxC inhibitors of the investigated series of *C*-glycosides, as well as **9**, serving as representative for the less active stereoisomers, were tested for their antibacterial activity on various bacterial strains, which presented either a defective efflux pump system or a decreased membrane permeability. Additionally, antimicrobial susceptibility testing was performed in the absence and the presence of phenylalanine-arginine- β -naphthylamide (PA β N) an inhibitor of efflux pumps belonging to the resistance-nodulation-division (RND) type (such as MexCD-OprJ in *P. aeruginosa* and AcrAB-TolC in *E. coli*).

All of the tested hydroxamic acids showed changes in their MIC values when tested against *E. coli* strains, which carry mutations affecting the intracellular concentration of small, hydrophilic compounds, such as antibiotics. These mutations are associated with either an increased intracellular drug concentration due to a reduced efflux in C600-R7 lacking OMP TolC of major tripartite RND efflux pump AcrAB-TolC or a reduced intracellular drug concentration due to a combined upregulation of AcrAB-TolC mediated efflux and simultaneous down-regulation of influx-mediating porin OmpF in *E. coli* WT-II.

Thus, all hydroxamic acids tested displayed higher antibiotic activity when assayed against *E. coli* C600-R7(Δ tolC) as compared to the parental *E. coli* C600 strain. On the contrary, mutant *E. coli* WT-II (Δ marR175) showed a decreased susceptibility for all hydroxamic acids assayed. The highest increase in antibiotic activity against *E. coli* C600-R7 (four serial dilution steps) as well as the highest decrease in antibiotic activity against *E. coli* WT-II (more than three serial dilution steps) were observed for *ent*-**8**, indicating that this compound is most affected by efflux pump systems. **8** showed the highest antibiotic activity of the investigated *C*-glycosides against all *E. coli* strains tested (Tables 1 and 3). **8** was in fact the only *C*-glycoside displaying antibacterial activity against the multidrug-resistant *E. coli* WT-II (Δ marR175) strain at 64 $\mu\text{g}\cdot\text{mL}^{-1}$, whereas its stereoisomers were not able to inhibit bacterial growth up to a concentration of 128 $\mu\text{g}\cdot\text{mL}^{-1}$. Interestingly, the MIC of **8** decreased only by one serial dilution step against the efflux-defective *E. coli* C600-R7 strain compared to the wild-type *E. coli* C600 strain. This suggests that the presence of efflux pumps has a minor effect on the potency of compound **8**. Together, these results show a varying degree of involvement of the major MDR efflux system AcrAB-TolC and/or the major porin OmpF in mediating a reduction of the intracellular concentration of the LpxC inhibitors.

E. coli type strains ATCC 25922 and ATCC 8739 are non-pathogenic susceptible strains used as control for determining antibacterial activity. The MIC values are within the range of one serial dilution step compared to *E. coli* C600 and *E. coli* WT [54], reflecting the natural degree of susceptibility of this species to the LpxC inhibitors tested.

Hydroxamic acid **8**, besides being the most active antibacterial compound against all *E. coli* strains screened, was also able to inhibit the growth of other Gram-negative bacterial strains, namely two *K.*

Table 3

MIC values in $\mu\text{g}\cdot\text{mL}^{-1}$ against various *E. coli*, *P. aeruginosa*, and *Klebsiella pneumoniae* strains. *(Δ MIC) indicates the change in serial dilutions steps between the MIC determined for the original wild-type strain and its mutated variant as well as between MIC determinations in the absence and presence of the efflux pump inhibitor PA β N (64 $\mu\text{g}\cdot\text{mL}^{-1}$). Increase and decrease in the MIC is indicated by a positive and a negative value, respectively. n.d.: not determined. **: clinical isolates.

Strain	<i>ent</i> - 8	8	9
	MIC [$\mu\text{g}\cdot\text{mL}^{-1}$] (Δ MIC)*		
<i>E. coli</i> C600	64	4	64
<i>E. coli</i> C600-R7 (Δ tolC)	4 (-4)	2 (-1)	8 (-3)
<i>E. coli</i> WT	32	16	128
<i>E. coli</i> WT-II (<i>AmarR175</i>)	>128 (\geq 3)	64 (2)	>128 (\geq 1)
<i>E. coli</i> ATCC 25922 (-PA β N)	16	4	32
<i>E. coli</i> ATCC 25922 (+PA β N)	n.d.	4 (0)	n.d.
<i>E. coli</i> ATCC 8739	32	16	64
<i>K. pneumoniae</i> 2941**	>128	32	n.d.
<i>K. pneumoniae</i> II-4.4**	64	16	n.d.
<i>P. aeruginosa</i> ML5087	>128	4	n.d.
<i>P. aeruginosa</i> ML5087 (<i>mexCD-oprJ</i>)	>128 (0)	4 (0)	n.d.
<i>P. aeruginosa</i> ATCC 27853 (-PA β N)	n.d.	16	n.d.
<i>P. aeruginosa</i> ATCC 27853 (+PA β N)	n.d.	2 (-3)	n.d.

pneumoniae clinical isolates, wild-type *P. aeruginosa* ML5087, and wild-type *P. aeruginosa* ATCC 27853. In contrast, its enantiomer *ent*-**8** was found to be inactive up to a concentration of 128 $\mu\text{g}\cdot\text{mL}^{-1}$ against *K. pneumoniae* 2941 and *P. aeruginosa* ML5087.

With a MIC value of 4 $\mu\text{g}\cdot\text{mL}^{-1}$, *C*-glycoside **8** showed promising antibacterial activity against the challenging wild-type *P. aeruginosa* ML5087 strain. The *nfxB* mutation of ML5087, leading to an over-expression of the MexCD-OprJ MDR efflux pump, had no impact on the activity of *C*-glycoside **8**, which might be explained by a lack of substrate specificity of the pump [55].

In order to further investigate the involvement of efflux pump systems in the inhibitory activity of compound **8**, two additional experiments including the efflux pump inhibitor PA β N were performed. When **8** was assayed against *E. coli* ATCC 25922 in the presence of PA β N, no change in the MIC value was observed compared to the experiment without the efflux pump inhibitor. This is in agreement with the results obtained for *E. coli* C600 and *E. coli* C600-R7, indicating that the efflux pump AcrAB-TolC has a minor effect on the antibacterial activity of **8** against *E. coli*. When assayed against *P. aeruginosa* ATCC 27853, a pronounced decrease in the MIC of **8** (three serial dilution steps) was observed in the presence of PA β N. Taken together with the results against *P. aeruginosa* ML5087-*nfxB*, this indicates that **8** is prone to efflux in *P. aeruginosa* but not substrate of MexCD-OprJ.

In order to assess the impact of efflux on the bacterial accumulation of **8**, we determined its quantity in the cytoplasm, periplasm, and membrane fractions in *E. coli* (BW25113) and the corresponding Δ tolC strain (JW5503-1) (Fig. 4). Bacteria were grown to an OD₆₀₀ of 0.8, incubated with a concentration of 100 $\text{ng}\cdot\text{mL}^{-1}$ of **8** for 10 min, fractionated using an osmotic shock and centrifugation steps according to an established protocol [56]. The concentration of **8** in the fractions was then determined by a liquid chromatography coupled to tandem mass spectrometry (LC/MS/MS). We observed an about 6-fold higher quantity of compound accumulated in the efflux-deficient strain compared with the wild-type strain. Furthermore, the majority of **8** (70% for the wild-type) was found in the cytoplasm, the target compartment of LpxC inhibitors, whereas 26% and 4% were located in membrane fractions. However, because the volume of the cytoplasm exceeds those of the periplasm and the membranes, the order of concentrations is different. The concentration in the periplasm is highest (18.9 $\text{pg}\cdot\mu\text{L}$), and lower, comparable concentrations are detected in the membrane fractions (4.8

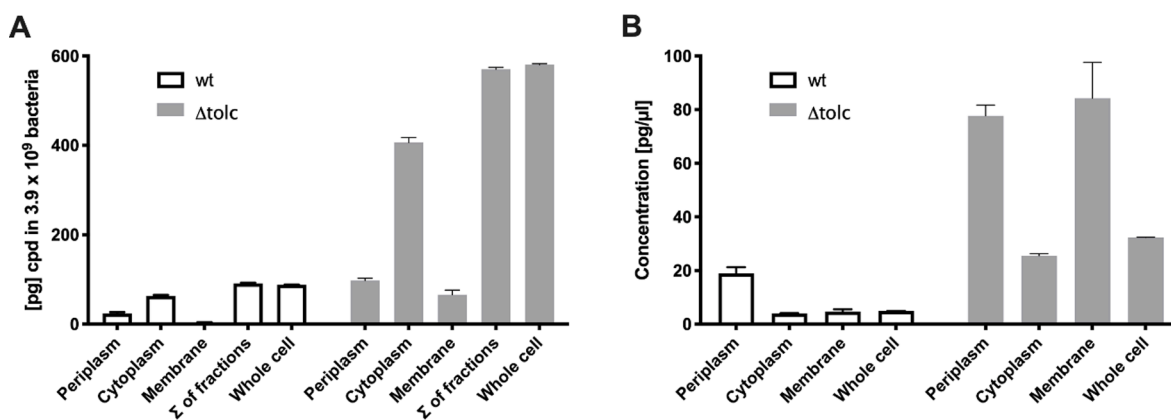


Fig. 4. Accumulation of **8** in *E. coli*. The quantities of **8**, expressed in pg per 3.9×10^9 bacteria (A) or as concentration in pg/ μL (B), in the periplasm, cytoplasm, and the membranes of two *E. coli* strains (BW25113 and its isogenic ΔtolC mutant), following a 10 min exposure of 100 ng/mL, are depicted.

pg/ μL) and the cytoplasm (4.0 pg/ μL). The accumulation data indicate that efflux plays a role in limiting the microbiological efficacy of **8**. The intracellular concentrations reached after short exposure of bacteria to 100 ng/mL are much lower than those required for LpxC binding, which in case of **8** is associated with a K_i of 0.4 μM . To enhance target engagement in the cell, the extracellular levels of **8** need to be increased, or compounds with an even higher bacterial permeability are required.

3. Summary and conclusions

A series of four 2*r*,3*c*,4*t*-configured *C*-furanosidic hydroxamic acids (**10**, **11**, *ent*-**10**, *ent*-**11**) was obtained in chiral pool syntheses starting from D- and L-xylose. The *C*-glycosidic scaffolds were established by reducing hemiketals **15** and *ent*-**15** with Et_3SiH in the presence of $\text{BF}_3 \cdot \text{OEt}_2$ yielding both anomeric *C*-aryl furanosides, each. The configuration of the newly established stereocenter could be unequivocally proven by X-ray crystallography.

The biological evaluation of the newly synthesized hydroxamic acids revealed that all of them exhibit inhibitory activity toward LpxC and antibacterial activity against the LpxC-defective *E. coli* D22 strain and, with the exception of *ent*-**10**, also against *E. coli* BL21(DE3). However, none of these *C*-furanosides was found to outperform their D-ribose-derived (2*S*,3*S*,4*R*,5*S*)-configured stereoisomer **8**.

Molecular docking studies were performed to rationalize the observed biological activities of the newly synthesized *C*-furanosides and their previously described stereoisomers. The (2*S*,3*S*,4*R*,5*S*)-configured *C*-furanoside **8**, the stereoisomer with the highest inhibitory activity toward LpxC, was found to adopt the most suitable conformation for ligand binding, both with respect to protein-ligand shape complementarity and hydrogen bond formation. The variation of the stereochemistry of compound **8** was found to cause a loss of key interactions with the enzyme accounting for the observed decline in inhibitory activity. However, a comparison of the available stereoisomers revealed that there is not one single stereocenter, which is obligatorily required to exhibit a certain configuration for high inhibitory activity, as among the most potent LpxC inhibitors (**8**, *ent*-**9**, *ent*-**8**, **7**, and **10**) all four stereocenters can be found in both configurations. Thus, apparently the interplay of the stereocenters needs to be considered.

To investigate whether the *C*-furanosidic LpxC inhibitors are able to cross the bacterial cell wall, thus reaching their cytoplasmic target, as well as to examine whether they are substrates of efflux pumps, the concentration of compound **8** in subcellular compartments of *E. coli* was determined and compounds **8**, *ent*-**8**, and **9** were tested for antibacterial activity on bacterial strains, which exhibit either a defective efflux pump system or a decreased membrane permeability. The antibacterial screening of the selected hydroxamic acids against the efflux impaired *E. coli* strain C600-R7 and the *E. coli* mutant WT-II, presenting a

combination of overexpression of major MDR efflux pump AcrAB-TolC and downregulation of influx-mediating porin OmpF, indicate an involvement of these factors in controlling the intracellular concentration of the compounds. Whereas the *tolC* mutant *E. coli* strain C600-R7 showed an increased susceptibility against the tested hydroxamic acids, the *marR* mutant *E. coli* strain WT-II exhibited a decreased susceptibility. Apparently, the hydroxamic acids are generally able to enter the bacterial cells, reaching the cytoplasm. However, they are substrates of the major efflux pump system AcrAB-TolC of *E. coli* and are extruded to the outside environment. *C*-glycoside **8**, the hydroxamic acid with the highest antibacterial activity of the investigated series of compounds, was found to be least prone to efflux by AcrAB-TolC, which was confirmed by control experiments with the efflux pump inhibitor PABN. Whereas the presence of PABN increased the antibacterial susceptibility of *P. aeruginosa* ATCC 27853, the *nfxB* mutation of *P. aeruginosa* ML5087 was found to have no impact on the antibacterial activity of *C*-glycoside **8** ($\text{MIC} = 4 \mu\text{g/mL}$), which indicates that **8** is prone to efflux but not substrate of the MexCD-OprJ MDR efflux pump.

The microbiological data obtained with the various *E. coli* strains were confirmed by accumulation experiments *E. coli* (BW25113) and the corresponding ΔtolC strain (JW5503-1), in which the concentration of compound **8** in the cytoplasm, periplasm, and membrane fractions was determined. The observed 6-fold higher concentration of hydroxamic acid **8** in the efflux-deficient strain compared to the wild-type strain additionally indicated that efflux plays a role in limiting the microbiological efficacy of the *C*-glycoside. Furthermore, the concentration in the cytoplasm of *E. coli* (BW25113) (4.0 pg/ μL) reached after a short exposure to **8** (100 ng/mL) was found to be much lower than the one required for LpxC inhibition, which is also in agreement with the determined MIC values. However, these data also indicate that in further optimization steps, the bacterial permeability of the *C*-glycosidic LpxC inhibitors needs to be increased.

4. Experimental section

4.1. Chemistry, general

All experiments involving water- or air-sensitive compounds were carried out under anhydrous conditions (N_2 atmosphere). Reagents were purchased from various suppliers and were used without further purification, unless otherwise noted. Anhydrous solvents were purchased from Acros Organics (extra dry over molecular sieves). Solvents for flash column chromatography were purchased in technical grade and distilled prior to use. Ultrapure water for reversed-phase chromatography was purified using a Sartorius arium® pro system (Sartopore 0.2 μm , UV). ACN for reversed-phase chromatography was purchased from VWR (HPLC grade). Flash column chromatography on silica gel was

performed using Macherey Nagel silica gel 60 M (0.040–0.063 mm). Parentheses include diameter of the column, fraction size, eluent and R_f value. Thin-layer chromatography was performed on Macherey Nagel precoated TLC sheets (ALUGRAM® Xtra SIL G/UV₂₅₄). Visualization was achieved by heat-staining using a cerium molybdate dipping bath [Ce(SO₄)₂ (1.8 g), (NH₄)₆Mo₇O₂₄ × 4 H₂O (45 g), conc. H₂SO₄ (45 g), H₂O (900 mL)]. Automatic reversed-phase flash column chromatography was performed using Biotage® SNAP KP-C18-HS 12 g columns on an Isolera™ One (Biotage®). Product-containing fractions were lyophilized using a Christ Alpha 2–4 LDplus freeze-dryer. Melting points were measured with a Büchi Melting Point M-565 and are uncorrected. Optical rotation α [deg] was determined with a P8000 polarimeter (A. Krüss Optronic GmbH); path length 1 dm, wavelength 589 nm (sodium D line); the unit of the specific rotation $[\alpha]_D^{20}$ [deg·mL·dm⁻¹·g⁻¹] is omitted; the concentration of the sample c [mg·mL⁻¹] and the solvent used are given in brackets. IR spectra were recorded on a Bruker Alpha FT-IR Platinum ATR spectro-photometer. NMR solvents were purchased from Eurisotop (CD₃OD) and Deutero (DMSO-*d*₆). NMR-spectra were recorded at room temperature on Bruker Avance I 400, DRX 500 and Avance III 600 instruments. High-resolution mass spectrometry was performed using an Agilent 6224 ESI-TOF instrument. HPLC methods for the determination of product purity: Method 1: VWR Hitachi equipment; UV/VIS detector: 5420; autosampler: 5260; pump: 5160; column: LiChrospher® 60 RP-select B (5 μ m); LiChroCART® 250–4 mm cartridge. flow rate: 1.00 mL/min; injection volume: 5.0 μ L; detection at λ = 210 nm for 30 min; solvents: A: water with 0.05% (V/V) trifluoroacetic acid; B: acetonitrile with 0.05% (V/V) trifluoroacetic acid; gradient elution: (A%): 0–4 min: 90%, 4–29 min: gradient from 90% to 0%, 29–31 min: 0%, 31–31.5 min: gradient from 0% to 90%, 31.5–40 min: 90%. Method 2: VWR Hitachi equipment; UV/VIS detector: 5420; autosampler: 5260; pump: 5160; column: phenomenex Gemini® 5 μ m C6-Phenyl 110 Å; LC Column 250 × 4.6 mm; flow rate: 1.00 mL/min; injection volume: 5.0 μ L; detection at λ = 254 nm for 20 min; solvents: A: acetonitrile: 10 mM ammonium formate = 10: 90 with 0.1% formic acid; B: acetonitrile: 10 mM ammonium formate = 90: 10 with 0.1% formic acid; gradient elution: (A%): 0–5 min: 100%, 5–12 min: gradient from 100% to 0%, 12–20 min: 0%, 20–22 min: gradient from 0% to 100%, 22–30 min: 100%. For both methods data were collected and evaluated by Chromaster software. The single crystal X-ray experiment was performed using a SuperNova four-circle diffractometer in Kappa geometry with 50 W Cu and Mo microfocustubes, an Atlas CCD detector (Rigaku Oxford Diffraction), and a Cryostream 700 Plus cooler (100 K–300 K, Oxford Cryosystems Ltd). Data collection, cell refinement, data reduction, and absorption correction were done using CrysAlis^{Pro} (Rigaku Oxford Diffraction). Absorption correction was done with *multi-scan* [57] or *gaussian* [58] methods. Determination and refinement of space group: GRAL (Rigaku Oxford Diffraction) and OLEX 2 [59]; structure solution: SHELXT [60] (dual-space algorithm) or SHELXS (structure-invariant direct method); full-matrix least-squares refinement done on F^2 : SHELXL [60]. Missing secondary atom sites were located from the difference Fourier map. Non-hydrogen atoms were refined using individual, anisotropic temperature factors. Heteroatom-bound hydrogen atoms were freely refined in their positions. Carbon atom-bound hydrogen atoms were positioned geometrically and refined riding on their respective parent atoms. $U_{iso}(H)$ was fixed at 1.5 (OH, CH₃) or 1.2 (all other H atoms) of the parent atom's U_{eq} isotropic displacement parameter. The fully refined data were reviewed using PLATON [61]. Supplementary crystallographic data for this compound **20** can be obtained free of charge from the Cambridge Crystallographic Data Centre at www.ccdc.cam.ac.uk under the deposition number CCDC-1990436.

4.2. Synthetic procedures

4.2.1. (2S,4aR,7R,7aR)-7-Hydroxy-2-phenyltetrahydro-6H-furo[3,2-d][1,3]dioxin-6-one (13)

K₂CO₃ (12 g, 84 mmol, 1.2 eq) was added in portions to a solution of D-xylose (11 g, 70 mmol) in water (50 mL). After cooling the solution to 0 °C, bromine (3.9 mL, 12 g, 77 mmol, 1.1 eq) was added slowly to the vigorously stirring solution. The reaction mixture was stirred for 30 min at 0 °C and for additional 90 min at ambient temperature. Then, formic acid (2 mL) was added, leading to the decolourisation of the solution after about 15 min, whereupon the solvent was evaporated *in vacuo*. The residue was dissolved in dry THF (100 mL), the mixture was cooled to 0 °C, and benzaldehyde (21 mL, 22 g, 210 mmol, 3 eq) and conc. H₂SO₄ (2 mL) were added. After stirring the mixture at ambient temperature overnight, it was carefully neutralized using a saturated aqueous solution of NaHCO₃ and extracted with ethyl acetate (2×). The combined organic layers were dried (Na₂SO₄), filtered, and the solvent was removed *in vacuo*. The residue was purified by flash column chromatography (\emptyset = 8 cm, h = 20 cm, V = 65 mL, petroleum ether/ethyl acetate = 1/1, R_f = 0.35) to give **13** as colorless solid (5.4 g, 23 mmol, 33% yield). m.p.: 122 °C; $[\alpha]_D^{20}$ = +60.5 (3.8, methanol); ¹H NMR (400 MHz, DMSO-*d*₆): δ [ppm] = 4.00 (d, J = 5.0 Hz, 1H, 7-H), 4.26 (dd, J = 13.7/2.0 Hz, 1H, 4-H), 4.40 (d, J = 13.7 Hz, 1H, 4-H), 4.59 (d, J = 2.3 Hz, 1H, 7a-H), 4.65–4.69 (m, 1H, 4a-H), 5.69 (s, 1H, 2-H), 6.69 (d, J = 5.0 Hz, 1H, OH), 7.34–7.42 (m, 5H, H_{phenyl}); ¹³C NMR (101 MHz, DMSO-*d*₆): δ [ppm] = 65.7 (1C, C-4), 72.7 (1C, C-7), 73.4 (1C, C-4a), 76.7 (1C, C-7a), 97.9 (1C, C-2), 126.0 (2C, C-2'_{phenyl}, C-6'_{phenyl}), 128.1 (2C, C-3'_{phenyl}, C-5'_{phenyl}), 129.0 (1C, C-4'_{phenyl}), 137.6 (1C, C-1'_{phenyl}), 175.3 (1C, C-6); IR (neat): ν [cm⁻¹] = 3331, 2924, 2853, 1758, 1392, 1192, 1128, 1075, 1057, 987, 929, 906, 835, 760, 748, 699, 642, 522, 462; HRMS (m/z): $[M + H]^+$ calcd for C₁₂H₁₃O₅: 237.0757, found: 237.0752; HPLC (method 1): t_R = 16.9 min, purity 99.4%.

4.2.2. (2S,4aR,7R,7aS)-7-(Methoxymethoxy)-2-phenyltetrahydro-6H-furo[3,2-d][1,3]dioxin-6-one (14)

Under N₂ atmosphere, a solution of **13** (3.7 g, 15 mmol) in dry THF (100 mL) was cooled to –20 °C, a 60% suspension of sodium hydride in paraffin oil (1.9 g, 46 mmol, 3.0 eq) was added in one portion, and the mixture was stirred for 15 min. Then chloromethyl methyl ether (3.5 mL, 3.7 g, 46 mmol, 3.0 eq) was added dropwise and the mixture was warmed to ambient temperature. After stirring the reaction mixture for additional 45 min, the mixture was carefully neutralized using a saturated aqueous solution of NaHCO₃ and extracted with ethyl acetate (2×). The combined organic layers were dried (Na₂SO₄), filtered, and the solvent was removed *in vacuo*. The residue was purified by flash column chromatography (\emptyset = 6 cm, h = 20 cm, V = 65 mL, petroleum ether/ethyl acetate = 3/1, R_f = 0.60) to give **14** as colorless solid (3.2 g, 11 mmol, 73% yield). m.p.: 84 °C; $[\alpha]_D^{20}$ = +92.3 (3.5, methanol); ¹H NMR (500 MHz, DMSO-*d*₆): δ [ppm] = 3.34 (s, 3H, OCH₃), 4.11 (s, 1H, 7-H), 4.29 (dd, J = 13.8/2.0 Hz, 1H, 4-H), 4.42 (d, J = 13.8 Hz, 1H, 4-H), 4.70–4.72 (m, 1H, 4a-H), 4.78 (d, J = 6.7 Hz, 1H, OCH₂OCH₃), 4.80–4.83 (m, 2H, OCH₂OCH₃ (1H), 7a-H), 5.72 (s, 1H, 2-H), 7.35–7.42 (m, 5H, H_{phenyl}); ¹³C NMR (126 MHz, DMSO-*d*₆): δ [ppm] = 55.5 (1C, OCH₃), 65.6 (1C, C-4), 73.9 (1C, C-4a), 74.7 (1C, C-7a), 76.4 (1C, C-7), 95.8 (1C, OCH₂OCH₃), 98.0 (1C, C-2), 126.0 (2C, C-2'_{phenyl}, C-6'_{phenyl}), 128.1 (2C, C-3'_{phenyl}, C-5'_{phenyl}), 129.0 (1C, C-4'_{phenyl}), 137.4 (1C, C-1'_{phenyl}), 173.1 (1C, C-6); IR (neat): ν [cm⁻¹] = 2949, 2900, 1777, 1404, 1189, 1129, 1103, 1036, 990, 939, 917, 826, 761, 718, 697, 641, 605, 523; HRMS (m/z): $[M + H]^+$ calcd for C₁₄H₁₇O₆: 281.1020, found: 281.1021; HPLC (method 1): t_R = 20.6 min, purity 99.1%.

4.2.3. (2S,4aR,7R,7aS)-6-(4-Iodophenyl)-7-(methoxymethoxy)-2-phenyltetrahydro-4H-furo[3,2-d][1,3]dioxin-6-ol (15)

Under N₂ atmosphere, a solution of 1,4-diiodobenzene (7.5 g, 23 mmol, 2.3 eq) in dry THF (100 mL) was cooled to –78 °C and a 1.6 M

solution of *n*-butyllithium in hexanes (12 mL, 20 mmol, 2.0 eq) was added in one portion. After stirring the mixture at $-78\text{ }^{\circ}\text{C}$ for 5 min, a solution of **14** (2.8 g, 9.9 mmol) in dry THF (20 mL) was added dropwise and the mixture was stirred for additional 15 min. Then the reaction mixture was warmed to ambient temperature, neutralized with a saturated aqueous solution of NaHCO_3 , and extracted with ethyl acetate (2 \times). The combined organic layers were dried (Na_2SO_4), filtered, and the solvent was removed *in vacuo*. The residue was purified by flash column chromatography ($\varnothing = 6\text{ cm}$, $h = 20\text{ cm}$, $V = 65\text{ mL}$, petroleum ether/ethyl acetate = 1/1, $R_f = 0.32$) to give **15** as colorless oil (2.4 g, 5.0 mmol, 50% yield). $[\alpha]_D^{20} = -32.7$ (3.6, methanol); ^1H NMR (500 MHz, $\text{DMSO}-d_6$): δ [ppm] = 3.28 (s, 3H, OCH_3), 3.90 (s, 1H, 7-H), 4.20–4.26 (m, 2H, 4-H (1H), 4a-H), 4.28–4.34 (m, 1H, 4-H), 4.49 (d, $J = 2.3\text{ Hz}$, 1H, 7a-H), 4.69 (d, $J = 6.7\text{ Hz}$, 1H, OCH_2OCH_3), 4.71 (d, $J = 6.7\text{ Hz}$, 1H, OCH_2OCH_3), 5.55 (s, 1H, 2-H), 6.60 (s, 1H, OH), 7.30–7.42 (m, 5H, H_{phenyl}), 7.42–7.48 (m, 2H, 2'- $\text{H}_{4\text{-iodophenyl}}$, 6'- $\text{H}_{4\text{-iodophenyl}}$), 7.67–7.72 (m, 2H, 3'- $\text{H}_{4\text{-iodophenyl}}$, 5'- $\text{H}_{4\text{-iodophenyl}}$); the spectrum shows the signals for two anomeric cyclic hemiacetals and the respective open-chain ketone in the ratio 5:3:1; the signals for the major anomer are given; ^{13}C NMR (126 MHz, $\text{DMSO}-d_6$): δ [ppm] = 55.2 (1C, OCH_3), 66.5 (1C, C-4), 71.2 (1C, C-4a), 80.7 (1C, C-7a), 85.7 (1C, C-7), 93.8 (1C, C-4'- iodophenyl), 95.6 (1C, OCH_2OCH_3), 98.8 (1C, C-2), 104.3 (1C, C-6), 126.3 (2C, C-2''- phenyl , C-6''- phenyl), 128.1 (2C, C-3''- phenyl , C-5''- phenyl), 128.75 (2C, C-2'- iodophenyl , C-6'- iodophenyl), 128.87 (1C, C-4''- phenyl), 136.4 (2C, C-3'- iodophenyl , C-5'- iodophenyl), 138.1 (1C, C-1''- phenyl), 144.3 (1C, C-1'- iodophenyl); the signals for the major anomer are given; IR (neat): ν [cm^{-1}] = 3481, 2923, 1390, 1207, 1086, 1060, 1026, 996, 972, 936, 916, 817, 752, 697; HRMS (m/z): $[\text{M}-\text{OH}]^+$ calcd for $\text{C}_{20}\text{H}_{20}\text{IO}_5$: 467.0350, found: 467.0363; HPLC (method 1): $t_R = 23.6\text{ min}$ (major anomer) and 25.0 min (minor anomer), ratio 2.5:1, overall purity 98.0%.

4.2.4. (2S,4aR,6S,7S,7aR)-6-(4-Iodophenyl)-2-phenyltetrahydro-4H-furo[3,2-d][1,3]dioxin-7-ol (**16**) and (2S,4aR,6R,7S,7aR)-6-(4-Iodophenyl)-2-phenyltetrahydro-4H-furo[3,2-d][1,3]dioxin-7-ol (**17**)

Under N_2 atmosphere, a solution of **15** (11 g, 23 mmol) in dry ACN (100 mL) was cooled to $-40\text{ }^{\circ}\text{C}$. Et_3SiH (11 mL, 8.0 g, 69 mmol, 3.0 eq) was added in one portion, followed by the dropwise addition of $\text{BF}_3 \cdot \text{Et}_2\text{O}$ (5.7 mL, 6.5 g, 46 mmol, 2.0 eq). After stirring the reaction mixture for 1 h at $-40\text{ }^{\circ}\text{C}$, it was warmed to ambient temperature, neutralized with a saturated aqueous solution of NaHCO_3 , and extracted with ethyl acetate (2 \times). The combined organic layers were dried (Na_2SO_4), filtered, and the solvent was removed *in vacuo*. The residue was dissolved in dry THF (50 mL). Benzaldehyde (7.0 mL, 7.3 g, 69 mmol, 3.0 eq) and conc. H_2SO_4 (1 mL) were added. After stirring the reaction mixture at ambient temperature overnight, it was neutralized with ethyl acetate (2 \times). The combined organic layers were dried (Na_2SO_4), filtered, and the solvent was removed *in vacuo*. The residue was purified by flash column chromatography ($\varnothing = 6\text{ cm}$, $h = 20\text{ cm}$, $V = 65\text{ mL}$, petroleum ether/ethyl acetate = 2/1) to give **17** ($R_f = 0.61$) as colorless solid (2.3 g, 5.3 mmol, 23% yield) and **16** ($R_f = 0.23$) as colorless solid (3.2 g, 7.6 mmol, 33% yield).

Analytical data of **16**: m.p.: $146\text{ }^{\circ}\text{C}$; $[\alpha]_D^{20} = -46.5$ (3.4, methanol); ^1H NMR (400 MHz, $\text{DMSO}-d_6$): δ [ppm] = 3.90–3.94 (m, 1H, 7-H), 4.04–4.08 (m, 1H, 4a-H), 4.22 (dd, $J = 13.0/1.9\text{ Hz}$, 1H, 4-H), 4.31 (d, $J = 2.3\text{ Hz}$, 1H, 7a-H), 4.34 (d, $J = 13.0\text{ Hz}$, 1H, 4-H), 4.74 (d, $J = 1.7\text{ Hz}$, 1H, 6-H), 5.54 (s, 1H, 2-H), 5.77 (d, $J = 4.1\text{ Hz}$, 1H, OH), 7.27–7.39 (m, 7H, 2'- $\text{H}_{4\text{-iodophenyl}}$, 6'- $\text{H}_{4\text{-iodophenyl}}$, 2''- H_{phenyl} , 3''- H_{phenyl} , 4''- H_{phenyl} , 5''- H_{phenyl} , 6''- H_{phenyl}), 7.64–7.70 (m, 2H, 3'- $\text{H}_{4\text{-iodophenyl}}$, 5'- $\text{H}_{4\text{-iodophenyl}}$); ^{13}C NMR (101 MHz, $\text{DMSO}-d_6$): δ [ppm] = 66.6 (1C, C-4), 73.4 (1C, C-4a), 82.1 (1C, C-7a), 82.6 (1C, C-7), 87.7 (1C, C-6), 92.8 (1C, C-4'- iodophenyl), 98.7 (1C, C-2), 126.3 (2C, C-2''- phenyl , C-6''- phenyl), 128.0 (2C, C-3''- phenyl , C-5''- phenyl), 128.5 (2C, C-2'- iodophenyl , C-6'- iodophenyl), 128.8 (1C, C-4''- phenyl), 136.6 (2C, C-3'- iodophenyl , C-5'- iodophenyl), 138.3

(1C, C-1''- phenyl), 141.3 (1C, C-1'- iodophenyl); IR (neat): ν [cm^{-1}] = 3416, 2909, 1484, 1452, 1393, 1334, 1128, 1085, 1056, 1001, 989, 915, 851, 799, 747, 697, 663, 519, 450; HRMS (m/z): $[\text{M} + \text{Na}]^+$ calcd for $\text{C}_{18}\text{H}_{17}\text{INaO}_4$: 447.0064, found: 447.0023; HPLC (method 1): $t_R = 22.7\text{ min}$, purity 97.4%.

Analytical data of **17**: m.p.: $189\text{ }^{\circ}\text{C}$; $[\alpha]_D^{20} = -71.4$ (2.9, methanol); ^1H NMR (400 MHz, $\text{DMSO}-d_6$): δ [ppm] = 4.10–4.18 (m, 2H, 4-H (1H), 7-H), 4.18–4.22 (m, 1H, 4a-H), 4.28 (d, $J = 12.8\text{ Hz}$, 1H, 4-H), 4.45–4.49 (m, 1H, 7a-H), 5.16 (d, $J = 4.1\text{ Hz}$, 1H, OH), 5.26 (d, $J = 3.1\text{ Hz}$, 1H, 6-H), 5.58 (s, 1H, 2-H), 7.13–7.21 (m, 2H, 2'- $\text{H}_{4\text{-iodophenyl}}$, 6'- $\text{H}_{4\text{-iodophenyl}}$), 7.33–7.42 (m, 3H, 3''- H_{phenyl} , 4''- H_{phenyl} , 5''- H_{phenyl}), 7.42–7.49 (m, 2H, 2''- H_{phenyl} , 6''- H_{phenyl}), 7.62–7.69 (m, 2H, 3'- $\text{H}_{4\text{-iodophenyl}}$, 5'- $\text{H}_{4\text{-iodophenyl}}$); ^{13}C NMR (101 MHz, $\text{DMSO}-d_6$): δ [ppm] = 67.5 (1C, C-4), 72.5 (1C, C-4a), 76.2 (1C, C-7), 81.4 (1C, C-7a), 83.4 (1C, C-6), 92.7 (1C, C-4'- iodophenyl), 97.9 (1C, C-2), 126.3 (2C, C-2''- phenyl , C-6''- phenyl), 128.1 (2C, C-3''- phenyl , C-5''- phenyl), 128.8 (1C, C-4''- phenyl), 129.7 (2C, C-2'- iodophenyl , C-6'- iodophenyl), 136.2 (2C, C-3'- iodophenyl , C-5'- iodophenyl), 138.4 (1C, C-1''- phenyl), 138.6 (1C, C-1'- iodophenyl); IR (neat): ν [cm^{-1}] = 3362, 2923, 1481, 1451, 1393, 1301, 1225, 1130, 1106, 1068, 998, 832, 783, 746, 697, 541, 470; HRMS (m/z): $[\text{M} + \text{Na}]^+$ calcd for $\text{C}_{18}\text{H}_{17}\text{INaO}_4$: 447.0064, found: 447.0063; HPLC (method 1) $t_R = 23.0\text{ min}$, purity 99.6%.

4.2.5. (2R,3R,4R,5S)-2-(Hydroxymethyl)-5-(4-iodophenyl) tetrahydrofuran-3,4-diol (**18**)

16 (3.5 g, 8.2 mmol) was dissolved in ACN (50 mL) and conc. HCl (2 mL) was added. The mixture was stirred at ambient temperature for 10 min, then neutralized with a saturated aqueous solution of NaHCO_3 , and extracted with ethyl acetate (2 \times). The combined organic layers were dried (Na_2SO_4), filtered, and the solvent was removed *in vacuo*. The residue was purified by flash column chromatography ($\varnothing = 4\text{ cm}$, $h = 20\text{ cm}$, $V = 30\text{ mL}$, ethyl acetate, $R_f = 0.28$) to give **18** as colorless solid (1.2 g, 3.7 mmol, 45% yield). m.p.: $135\text{ }^{\circ}\text{C}$; $[\alpha]_D^{20} = -14.6$ (3.4, methanol); ^1H NMR (500 MHz, $\text{DMSO}-d_6$): δ [ppm] = 3.58–3.65 (m, 1H, CH_2OH), 3.68–3.77 (m, 2H, CH_2OH (1H), 4-H), 3.92–3.99 (m, 2H, 3-H, 2-H), 4.46 (d, $J = 4.0\text{ Hz}$, 1H, 5-H), 4.55 (t, $J = 5.7\text{ Hz}$, 1H, CH_2OH), 4.92 (d, $J = 4.1\text{ Hz}$, 1H, 3-OH), 5.43 (d, $J = 4.7\text{ Hz}$, 1H, 4-OH), 7.18–7.23 (m, 2H, 2'- $\text{H}_{4\text{-iodophenyl}}$, 6'- $\text{H}_{4\text{-iodophenyl}}$), 7.65–7.69 (m, 2H, 3'- $\text{H}_{4\text{-iodophenyl}}$, 5'- $\text{H}_{4\text{-iodophenyl}}$); ^{13}C NMR (126 MHz, $\text{DMSO}-d_6$): δ [ppm] = 59.8 (1C, CH_2OH), 77.4 (1C, C-3), 82.1 (1C, C-2), 84.4 (1C, C-4), 85.8 (1C, C-5), 92.7 (1C, C-4'- iodophenyl), 128.6 (2C, C-2'- iodophenyl , C-6'- iodophenyl), 136.6 (2C, C-3'- iodophenyl , C-5'- iodophenyl), 141.6 (1C, C-1'- iodophenyl); IR (neat): ν [cm^{-1}] = 3320, 2954, 2916, 1481, 1422, 1397, 1247, 1228, 1093, 1035, 998, 965, 837, 789, 740, 562, 521; HRMS (m/z): $[\text{M} + \text{Na}]^+$ calcd for $\text{C}_{11}\text{H}_{13}\text{INaO}_4$: 358.9751, found: 358.9747; HPLC (method 1): $t_R = 14.8\text{ min}$, purity 99.8%.

4.2.6. (2R,3R,4R,5R)-2-(Hydroxymethyl)-5-(4-iodophenyl) tetrahydrofuran-3,4-diol (**19**)

17 (2.3 g, 5.3 mmol) was dissolved in ACN (50 mL) and conc. HCl (2 mL) was added. The mixture was stirred at ambient temperature for 10 min, then neutralized with a saturated aqueous solution of NaHCO_3 , and extracted with ethyl acetate (2 \times). The combined organic layers were dried (Na_2SO_4), filtered, and the solvent was removed *in vacuo*. The residue was purified by flash column chromatography ($\varnothing = 4\text{ cm}$, $h = 20\text{ cm}$, $V = 30\text{ mL}$, ethyl acetate, $R_f = 0.29$) to give **19** as colorless solid (900 mg, 2.7 mmol, 50% yield). m.p.: $131\text{ }^{\circ}\text{C}$; $[\alpha]_D^{20} = -68.0$ (3.5, methanol); ^1H NMR (400 MHz, $\text{DMSO}-d_6$): δ [ppm] = 3.50–3.59 (m, 1H, CH_2OH), 3.59–3.67 (m, 1H, CH_2OH), 3.92–3.97 (m, 1H, 4-H), 4.03–4.07 (m, 1H, 3-H), 4.17 (td, $J = 6.0/3.4\text{ Hz}$, 1H, 2-H), 4.53 (t, $J = 5.7\text{ Hz}$, 1H, CH_2OH), 4.83 (d, $J = 4.6\text{ Hz}$, 1H, 4-OH), 4.98 (d, $J = 3.2\text{ Hz}$, 1H, 5-H), 5.14 (d, $J = 4.2\text{ Hz}$, 1H, 3-OH), 7.07–7.15 (m, 2H, 2'- $\text{H}_{4\text{-iodophenyl}}$, 6'- $\text{H}_{4\text{-iodophenyl}}$), 7.60–7.68 (m, 2H, 3'- $\text{H}_{4\text{-iodophenyl}}$, 5'- $\text{H}_{4\text{-iodophenyl}}$); ^{13}C NMR (101 MHz, $\text{DMSO}-d_6$): δ [ppm] = 59.8 (1C, CH_2OH), 76.7 (1C, C-3), 78.3 (1C, C-4), 81.4 (1C, C-5), 81.8 (1C, C-2), 92.4 (1C, C-4'- iodophenyl), 129.7

(2C, C-2'4-iodophenyl, C-6'4-iodophenyl), 136.1 (2C, C-3'4-iodophenyl, C-5'4-iodophenyl), 139.2 (1C, C-1'4-iodophenyl); IR (neat): ν [cm^{-1}] = 3301, 2938, 2903, 1481, 1403, 1228, 1202, 1102, 1075, 1061, 1046, 1034, 1005, 982, 766, 613, 527, 453; HRMS (m/z): $[\text{M} + \text{Na}]^+$ calcd for $\text{C}_{11}\text{H}_{13}\text{I}\text{NaO}_4$: 358.9751, found: 358.9730; HPLC (method 1): $t_{\text{R}} = 14.4$ min, purity 97.6%.

4.2.7. Methyl (2S,3R,4R,5S)-3,4-dihydroxy-5-(4-iodophenyl) tetrahydrofuran-2-carboxylate (20)

18 (490 mg, 1.4 mmol), TEMPO (250 mg, 1.6 mmol, 1.1 eq) and NCS (770 mg, 5.8 mmol, 4.0 eq) were dissolved in a mixture of ACN and a saturated aqueous solution of NaHCO_3 (1/1, 50 mL). The reaction mixture was stirred at 50 °C for 2 h, then acidified with conc. HCl to pH 1, and extracted with ethyl acetate (2 \times). The combined organic layers were dried (Na_2SO_4), filtered, and the solvent was removed *in vacuo*. The residue was dissolved in methanol (50 mL) and *p*-toluenesulfonic acid monohydrate (410 mg, 2.2 mmol, 1.5 eq) was added. The reaction mixture was heated to reflux overnight. Afterwards, a saturated aqueous solution of NaHCO_3 was added and the mixture was extracted with ethyl acetate (2 \times). The combined organic layers were dried (Na_2SO_4), filtered, and the solvent was removed *in vacuo*. The residue was purified by flash column chromatography ($\varnothing = 3$ cm, $h = 15$ cm, $V = 30$ mL, petroleum ether/ethyl acetate = 1/2, $R_{\text{f}} = 0.35$) to give **20** as colorless solid (280 mg, 0.76 mmol, 53% yield). m.p.: 181 °C; $[\alpha]_{\text{D}}^{20} = -4.8$ (5.0, methanol); ^1H NMR (400 MHz, $\text{DMSO}-d_6$): δ [ppm] = 3.67 (s, 3H, CO_2CH_3), 3.82–3.86 (m, 1H, 4-H), 4.17–4.22 (m, 1H, 3-H), 4.64 (d, $J = 4.2$ Hz, 1H, 5-H), 4.66 (d, $J = 5.3$ Hz, 1H, 2-H), 5.50 (d, $J = 4.4$ Hz, 1H, 3-OH), 5.62 (d, $J = 4.7$ Hz, 1H, 4-OH), 7.29–7.35 (m, 2H, 2'-H₄-iodophenyl, 6'-H₄-iodophenyl), 7.66–7.72 (m, 2H, 3'-H₄-iodophenyl, 5'-H₄-iodophenyl); ^{13}C NMR (101 MHz, $\text{DMSO}-d_6$): δ [ppm] = 51.4 (1C, CO_2CH_3), 77.9 (1C, C-3), 80.4 (1C, C-2), 82.5 (1C, C-4), 85.9 (1C, C-5), 93.0 (1C, C-4'4-iodophenyl), 128.7 (2C, C-2'4-iodophenyl, C-6'4-iodophenyl), 136.6 (2C, C-3'4-iodophenyl, C-5'4-iodophenyl), 140.8 (1C, C-1'4-iodophenyl), 169.9 (1C, CO_2CH_3); IR (neat): ν [cm^{-1}] = 3147, 3073, 2956, 2792, 1770, 1684, 1371, 1292, 1185, 1003, 935, 848, 816, 638, 556, 419; HRMS (m/z): $[\text{M} + \text{Na}]^+$ calcd for $\text{C}_{12}\text{H}_{13}\text{I}\text{NaO}_5$: 386.9700, found: 386.9703; HPLC (method 1): $t_{\text{R}} = 17.4$ min, purity 96.3%; X-ray crystal structure analysis: structural data can be found on <https://www.ccdc.cam.ac.uk> under the deposition number CCDC-1990436.

4.2.8. Methyl (2S,3R,4R,5R)-3,4-dihydroxy-5-(4-iodophenyl) tetrahydrofuran-2-carboxylate (21)

DMP (520 mg, 1.2 mmol, 2.0 eq) was added to a solution of **19** (200 mg, 0.61 mmol) in ACN (50 mL) and the mixture was stirred at ambient temperature for 30 min. Then, a saturated aqueous solution of NaHCO_3 was added and the mixture was extracted with ethyl acetate (2 \times). The combined organic layers were dried (Na_2SO_4), filtered, and the solvent was removed *in vacuo*. The residue was dissolved in a mixture of ACN (25 mL) and a solution of AgNO_3 (210 mg, 1.2 mmol, 2.0 eq) in water (25 mL). A 1 M aqueous solution of KOH (2.4 mL, 2.4 mmol, 4.0 eq) was added dropwise and the mixture was stirred at ambient temperature for 30 min, then acidified with conc. HCl to pH 1, and extracted with ethyl acetate (2 \times). The combined organic layers were dried (Na_2SO_4), filtered, and the solvent was removed *in vacuo*. The residue was dissolved in methanol (50 mL) and *p*-toluenesulfonic acid monohydrate (170 mg, 0.91 mmol, 1.5 eq) was added. The reaction mixture was heated to reflux overnight. Afterwards a saturated aqueous solution of NaHCO_3 was added and the mixture was extracted with ethyl acetate (2 \times). The combined organic layers were dried (Na_2SO_4), filtered, and the solvent was removed *in vacuo*. The residue was purified by flash column chromatography ($\varnothing = 3$ cm, $h = 15$ cm, $V = 30$ mL, petroleum ether/ethyl acetate = 1/2, $R_{\text{f}} = 0.32$) to give **21** as colorless solid (97 mg, 0.27 mmol, 44% yield). m.p.: 183 °C; $[\alpha]_{\text{D}}^{20} = -72.7$ (3.7, methanol); ^1H NMR (500 MHz, $\text{DMSO}-d_6$): δ [ppm] = 3.64 (s, 3H, CO_2CH_3), 3.93–3.98 (m, 1H, 4-H), 4.29–4.33 (m, 1H, 3-H), 4.81 (d, $J = 4.3$ Hz, 1H,

2-H), 5.06 (d, $J = 4.8$ Hz, 1H, 4-OH), 5.10 (d, $J = 2.8$ Hz, 1H, 5-H), 5.71–5.73 (m, 1H, 3-OH), 7.11–7.16 (m, 2H, 2'-H₄-iodophenyl, 6'-H₄-iodophenyl), 7.64–7.68 (m, 2H, 3'-H₄-iodophenyl, 5'-H₄-iodophenyl); ^{13}C NMR (151 MHz, $\text{DMSO}-d_6$): δ [ppm] = 51.3 (1C, CO_2CH_3), 77.8 (1C, C-4), 78.2 (1C, C-3), 80.7 (1C, C-2), 82.7 (1C, C-5), 92.8 (1C, C-4'4-iodophenyl), 129.6 (2C, C-2'4-iodophenyl, C-6'4-iodophenyl), 136.2 (2C, C-3'4-iodophenyl, C-5'4-iodophenyl), 137.7 (1C, C-1'4-iodophenyl), 170.2 (1C, CO_2CH_3); IR (neat): ν [cm^{-1}] = 3399, 2951, 2925, 2852, 1739, 1485, 1440, 1365, 1222, 1055, 1006, 772, 731, 477, 451; HRMS (m/z): $[\text{M} + \text{Na}]^+$ calcd for $\text{C}_{12}\text{H}_{13}\text{I}\text{NaO}_5$: 386.9700, found: 386.9693; HPLC (method 1): $t_{\text{R}} = 16.8$ min, purity 96.1%.

4.2.9. Methyl (2S,3R,4R,5S)-3,4-dihydroxy-5-(4-([4-(morpholinomethyl)phenyl]ethynyl)phenyl)tetrahydrofuran-2-carboxylate (22)

Under N_2 atmosphere, copper(I) iodide (13 mg, 0.066 mmol, 0.2 eq), tetrakis(triphenylphosphine)palladium(0) (38 mg, 0.033 mmol, 0.1 eq) and triethylamine (0.3 mL, 240 mg, 2.3 mmol, 7.0 eq) were added to a solution of **20** (120 mg, 0.33 mmol) in dry ACN (40 mL). Then, a solution of 4-(morpholinomethyl)phenylacetylene (100 mg, 0.50 mmol, 1.5 eq) in dry ACN (5 mL) was added dropwise over a period of 30 min at ambient temperature. Afterwards, the solvent was removed *in vacuo* and the residue was purified by flash column chromatography ($\varnothing = 3$ cm, $h = 15$ cm, $V = 30$ mL, CH_2Cl_2 /methanol = 19/1, $R_{\text{f}} = 0.32$) to give **22** as colorless solid (70 mg, 0.16 mmol, 48% yield). m.p.: 151 °C; $[\alpha]_{\text{D}}^{20} = -34.4$ (3.6, methanol); ^1H NMR (600 MHz, $\text{DMSO}-d_6$): δ [ppm] = 2.31–2.39 (m, 4H, $\text{NCH}_2\text{CH}_2\text{O}$), 3.49 (s, 2H, ArCH_2N), 3.55–3.60 (m, 4H, $\text{NCH}_2\text{CH}_2\text{O}$), 3.69 (s, 3H, CO_2CH_3), 3.86–3.90 (m, 1H, 4-H), 4.20–4.24 (m, 1H, 3-H), 4.68 (d, $J = 5.2$ Hz, 1H, 2-H), 4.70 (d, $J = 4.3$ Hz, 1H, 5-H), 5.52 (d, $J = 4.4$ Hz, 1H, 3-OH), 5.65 (d, $J = 4.8$ Hz, 1H, 4-OH), 7.33–7.38 (m, 2H, 3''-H₄-(morpholinomethyl)phenyl, 5''-H₄-(morpholinomethyl)phenyl), 7.48–7.53 (m, 4H, 2''-H₄-(morpholinomethyl)phenyl, 6''-H₄-(morpholinomethyl)phenyl, 3'-H₄-{[4-(morpholinomethyl)phenyl]ethynyl}phenyl, 5'-H₄-{[4-(morpholinomethyl)phenyl]ethynyl}phenyl), 7.53–7.57 (m, 2H, 2'-H₄-{[4-(morpholinomethyl)phenyl]ethynyl}phenyl, 6'-H₄-{[4-(morpholinomethyl)phenyl]ethynyl}phenyl); ^{13}C NMR (151 MHz, $\text{DMSO}-d_6$): δ [ppm] = 51.4 (1C, CO_2CH_3), 53.2 (2C, $\text{NCH}_2\text{CH}_2\text{O}$), 62.0 (1C, ArCH_2N), 66.2 (2C, $\text{NCH}_2\text{CH}_2\text{O}$), 77.9 (1C, C-3), 80.4 (1C, C-2), 82.6 (1C, C-4), 86.1 (1C, C-5), 89.0 (1C, $\text{C}\equiv\text{C}$), 89.2 (1C, $\text{C}\equiv\text{C}$), 120.9 (1C, C-1'4-(morpholinomethyl)phenyl), 121.0 (1C, C-4'4-{[4-(morpholinomethyl)phenyl]ethynyl}phenyl), 126.7 (2C, C-2'4-{[4-(morpholinomethyl)phenyl]ethynyl}phenyl, C-6'4-{[4-(morpholinomethyl)phenyl]ethynyl}phenyl), 129.2 (2C, C-3''4-(morpholinomethyl)phenyl, C-5''4-(morpholinomethyl)phenyl), 130.9 (2C, C-3'4-{[4-(morpholinomethyl)phenyl]ethynyl}phenyl, C-5'4-{[4-(morpholinomethyl)phenyl]ethynyl}phenyl), 131.2 (2C, C-2''4-(morpholinomethyl)phenyl, C-6''4-(morpholinomethyl)phenyl), 138.8 (1C, C-4''4-(morpholinomethyl)phenyl), 141.7 (1C, C-1'4-{[4-(morpholinomethyl)phenyl]ethynyl}phenyl), 169.9 (1C, CO_2CH_3); IR (neat): ν [cm^{-1}] = 3372, 2924, 2856, 2814, 1740, 1518, 1439, 1350, 1292, 1209, 1106, 1047, 1003, 862, 831, 793, 530; HRMS (m/z): $[\text{M} + \text{H}]^+$ calcd for $\text{C}_{25}\text{H}_{28}\text{NO}_6$: 438.1911, found: 438.1908; HPLC (method 1): $t_{\text{R}} = 14.7$ min, purity 96.4%.

4.2.10. Methyl (2S,3R,4R,5R)-3,4-dihydroxy-5-(4-([4-(morpholinomethyl)phenyl]ethynyl)phenyl)tetrahydrofuran-2-carboxylate (23)

Under N_2 atmosphere, copper(I) iodide (13 mg, 0.070 mmol, 0.2 eq), tetrakis(triphenylphosphine)palladium(0) (41 mg, 0.035 mmol, 0.1 eq) and triethylamine (0.34 mL, 250 mg, 2.5 mmol, 7.0 eq) were added to a solution of **21** (130 mg, 0.35 mmol) in dry ACN (40 mL). Then a solution of 4-(morpholinomethyl)phenylacetylene (110 mg, 0.53 mmol, 1.5 eq) in dry ACN (5 mL) was added dropwise over a period of 30 min at ambient temperature. Afterwards, the solvent was removed *in vacuo* and the residue was purified by flash column chromatography ($\varnothing = 3$ cm, $h = 15$ cm, $V = 30$ mL, CH_2Cl_2 /methanol = 19/1, $R_{\text{f}} = 0.33$) to give **23** as colorless solid (100 mg, 0.24 mmol, 68% yield). m.p.: 212 °C; $[\alpha]_{\text{D}}^{20} = -89.7$ (3.2, methanol); ^1H NMR (600 MHz, $\text{DMSO}-d_6$): δ [ppm] = 2.31–2.39 (m, 4H, $\text{NCH}_2\text{CH}_2\text{O}$), 3.49 (s, 2H, ArCH_2N), 3.55–3.60 (m,

4H, NCH₂CH₂O), 3.65 (s, 3H, CO₂CH₃), 3.99–4.03 (m, 1H, 4-H), 4.32–4.35 (m, 1H, 3-H), 4.84 (d, *J* = 4.3 Hz, 1H, 2-H), 5.09 (d, *J* = 4.8 Hz, 1H, 4-OH), 5.17 (d, *J* = 2.8 Hz, 1H, 5-H), 5.75 (d, *J* = 4.7 Hz, 1H, 3-OH), 7.33–7.39 (m, 4H, 3''-H₄-(morpholinomethyl)phenyl, 5''-H₄-(morpholinomethyl)phenyl, 2''-H₄-{[4-(morpholinomethyl)phenyl]ethynyl}phenyl, 6''-H₄-{[4-(morpholinomethyl)phenyl]ethynyl}phenyl), 7.46–7.52 (m, 4H, 2''-H₄-(morpholinomethyl)phenyl, 6''-H₄-(morpholinomethyl)phenyl, 3''-H₄-{[4-(morpholinomethyl)phenyl]ethynyl}phenyl, 5''-H₄-{[4-(morpholinomethyl)phenyl]ethynyl}phenyl); ¹³C NMR (151 MHz, DMSO-*d*₆): δ [ppm] = 51.3 (1C, CO₂CH₃), 53.2 (2C, NCH₂CH₂O), 62.0 (1C, ArCH₂N), 66.2 (2C, NCH₂CH₂O), 77.9 (1C, C-4), 78.3 (1C, C-3), 80.7 (1C, C-2), 82.9 (1C, C-5), 89.0 (1C, C≡C), 89.3 (1C, C≡C), 120.8 (1C, C-4'-{[4-(morpholinomethyl)phenyl]ethynyl}phenyl), 121.0 (1C, C-1''-4-(morpholinomethyl)phenyl), 127.6 (2C, C-2''-4-{[4-(morpholinomethyl)phenyl]ethynyl}phenyl, C-6''-4-{[4-(morpholinomethyl)phenyl]ethynyl}phenyl), 129.2 (2C, C-3''-4-(morpholinomethyl)phenyl, C-5''-4-(morpholinomethyl)phenyl), 130.6 (2C, Carom.), 131.2 (2C, Carom.), 138.7 (2C, C-4''-4-(morpholinomethyl)phenyl, C-1''-4-{[4-(morpholinomethyl)phenyl]ethynyl}phenyl), 170.3 (1C, CO₂CH₃); IR (neat): ν [cm⁻¹] = 3399, 2925, 2853, 2801, 1735, 1518, 1436, 1367, 1349, 1292, 1229, 1119, 1085, 1058, 1007, 868, 842, 783, 583; HRMS (*m/z*): [M + H]⁺ calcd for C₂₅H₂₈NO₆: 438.1911, found: 438.1910; HPLC (method 1): t_R = 14.3 min, purity 98.7%.

4.2.11. (2*S*,3*R*,4*R*,5*S*)-*N*,3,4-Trihydroxy-5-(4-{[4-(morpholinomethyl)phenyl]ethynyl}phenyl)tetrahydrofuran-2-carboxamide (10)

Under N₂ atmosphere, hydroxylamine hydrochloride (790 mg, 11 mmol, 100 eq) and a 5.4 M solution of sodium methoxide in methanol (2.1 mL, 11 mmol, 100 eq) were added to a solution of **22** (50 mg, 0.11 mmol) in dry methanol (20 mL) and the mixture was stirred at ambient temperature overnight. After filtration, the solvent was removed *in vacuo*. The residue was purified by automatic flash column chromatography (5% → 100% ACN in H₂O, Biotage® SNAP KP-C18-HS 12 g) to give **10** as colorless solid (26 mg, 0.059 mmol, 52% yield). m.p. = 178 °C (decomposition); [α]_D²⁰ = -30.7 (2.8, methanol); ¹H NMR (600 MHz, DMSO-*d*₆): δ [ppm] = 2.31–2.39 (m, 4H, NCH₂CH₂O), 3.49 (s, 2H, NCH₂Ar), 3.55–3.59 (m, 4H, NCH₂CH₂O), 3.77–3.80 (m, 1H, 4-H), 3.88–3.91 (m, 1H, 3-H), 4.10 (d, *J* = 3.2 Hz, 1H, 2-H), 4.59 (d, *J* = 2.3 Hz, 1H, 5-H), 5.38 (s br, 1H, 4-OH), 7.32–7.37 (m, 2H, 3''-H₄-(morpholinomethyl)phenyl, 5''-H₄-(morpholinomethyl)phenyl), 7.44–7.48 (m, 2H, 3''-H₄-{[4-(morpholinomethyl)phenyl]ethynyl}phenyl, 5''-H₄-{[4-(morpholinomethyl)phenyl]ethynyl}phenyl), 7.48–7.51 (m, 2H, 2''-H₄-(morpholinomethyl)phenyl, 6''-H₄-(morpholinomethyl)phenyl), 7.51–7.54 (m, 2H, 2''-H₄-{[4-(morpholinomethyl)phenyl]ethynyl}phenyl, 6''-H₄-{[4-(morpholinomethyl)phenyl]ethynyl}phenyl), 7.80 (s br, 1H, NHOH), 7.94 (s br, 1H, NHOH); ¹³C NMR (151 MHz, DMSO-*d*₆): δ [ppm] = 53.2 (2C, NCH₂CH₂O), 62.0 (1C, NCH₂Ar), 66.2 (2C, NCH₂CH₂O), 78.5 (1C, C-2), 79.9 (1C, C-3), 84.4 (1C, C-4), 87.2 (1C, C-5), 88.8 (1C, C≡C), 89.4 (1C, C≡C), 120.5 (1C, C-4'-{[4-(morpholinomethyl)phenyl]ethynyl}phenyl), 121.0 (1C, C-1''-4-(morpholinomethyl)phenyl), 126.8 (2C, C-2''-4-{[4-(morpholinomethyl)phenyl]ethynyl}phenyl, C-6''-4-{[4-(morpholinomethyl)phenyl]ethynyl}phenyl), 129.2 (2C, C-3''-4-(morpholinomethyl)phenyl, C-5''-4-(morpholinomethyl)phenyl), 130.8 (2C, C-3'-4-{[4-(morpholinomethyl)phenyl]ethynyl}phenyl, C-5'-4-{[4-(morpholinomethyl)phenyl]ethynyl}phenyl), 131.2 (2C, C-2''-4-(morpholinomethyl)phenyl, C-6''-4-(morpholinomethyl)phenyl), 138.7 (1C, C-4''-4-(morpholinomethyl)phenyl), 143.3 (1C, C-1''-4-{[4-(morpholinomethyl)phenyl]ethynyl}phenyl), 164.5 (1C, C=O); IR (neat): ν [cm⁻¹] = 3223, 2811, 1626, 1516, 1429, 1350, 1290, 1109, 1048, 1006, 865, 830; HRMS (*m/z*): [M + H]⁺ calcd for C₂₄H₂₇N₂O₆: 439.1864, found: 439.1860; HPLC (method 2): t_R = 12.0 min, purity 99.7%.

4.2.12. (2*S*,3*R*,4*R*,5*R*)-*N*,3,4-Trihydroxy-5-(4-{[4-(morpholinomethyl)phenyl]ethynyl}phenyl)tetrahydrofuran-2-carboxamide (11)

Under N₂ atmosphere, hydroxylamine hydrochloride (1.1 g, 15 mmol, 100 eq) and a 5.4 M solution of sodium methoxide in methanol (2.8 mL, 15 mmol, 100 eq) were added to a solution of **23** (67 mg, 0.15 mmol) in dry methanol (20 mL) and the mixture was stirred at ambient temperature overnight. After filtration, the solvent was removed *in*

vacuo. The residue was purified by automatic flash column chromatography (5% → 100% ACN in H₂O, Biotage® SNAP KP-C18-HS 12 g) to give **11** as colorless solid (12 mg, 0.027 mmol, 18% yield). m.p. = 174 °C (decomposition); [α]_D²⁰ = -109.1 (2.2, methanol); ¹H NMR (600 MHz, DMSO-*d*₆): δ [ppm] = 2.31–2.39 (m, 4H, NCH₂CH₂O), 3.49 (s, 2H, NCH₂Ar), 3.55–3.60 (m, 4H, NCH₂CH₂O), 3.94–3.98 (m, 1H, 4-H), 4.06–4.09 (m, 1H, 3-H), 4.25–4.28 (m, 1H, 2-H), 4.75 (s br, 1H, OH), 5.18 (d, *J* = 3.1 Hz, 1H, 5-H), 7.32–7.37 (m, 4H, 3''-H₄-(morpholinomethyl)phenyl, 5''-H₄-(morpholinomethyl)phenyl, 2''-H₄-{[4-(morpholinomethyl)phenyl]ethynyl}phenyl, 6''-H₄-{[4-(morpholinomethyl)phenyl]ethynyl}phenyl), 7.43–7.48 (m, 2H, 3''-H₄-{[4-(morpholinomethyl)phenyl]ethynyl}phenyl, 5''-H₄-{[4-(morpholinomethyl)phenyl]ethynyl}phenyl), 7.48–7.52 (m, 2H, 2''-H₄-(morpholinomethyl)phenyl, 6''-H₄-(morpholinomethyl)phenyl), 7.97 (s br, 2H, NHOH); ¹³C NMR (151 MHz, DMSO-*d*₆): δ [ppm] = 53.2 (2C, NCH₂CH₂O), 62.0 (1C, NCH₂Ar), 66.2 (2C, NCH₂CH₂O), 78.0 (1C, C-2), 78.4 (1C, C-4), 79.2 (1C, C-3), 82.5 (1C, C-5), 88.7 (1C, C≡C), 89.5 (1C, C≡C), 120.3 (1C, C-4'-{[4-(morpholinomethyl)phenyl]ethynyl}phenyl), 121.1 (1C, C-1''-4-(morpholinomethyl)phenyl), 127.6 (2C, C-2''-4-{[4-(morpholinomethyl)phenyl]ethynyl}phenyl, C-6''-4-{[4-(morpholinomethyl)phenyl]ethynyl}phenyl), 129.2 (2C, C-3''-4-(morpholinomethyl)phenyl, C-5''-4-(morpholinomethyl)phenyl), 130.4 (2C, C-3'-4-{[4-(morpholinomethyl)phenyl]ethynyl}phenyl, C-5'-4-{[4-(morpholinomethyl)phenyl]ethynyl}phenyl), 131.2 (2C, C-2''-4-(morpholinomethyl)phenyl, C-6''-4-(morpholinomethyl)phenyl), 138.7 (1C, C-4''-4-(morpholinomethyl)phenyl), 140.5 (1C, C-1''-4-{[4-(morpholinomethyl)phenyl]ethynyl}phenyl), 165.2 (1C, C=O); IR (neat): ν [cm⁻¹] = 3299, 2919, 2857, 2811, 1630, 1517, 1455, 1369, 1352, 1292, 1109, 1082, 1063, 1006, 863, 824, 790, 763; HRMS (*m/z*): [M + H]⁺ calcd for C₂₄H₂₇N₂O₆: 439.1864, found: 439.1862; HPLC (method 2): t_R = 11.8 min, purity 99.1%.

4.3. Biological evaluation

4.3.1. Disk diffusion assay

The antibiotic activity of the synthesized inhibitors was determined by disk diffusion assays. Liquid cultures of *E. coli* BL21(DE3) and the defective strain *E. coli* D22 [47] were grown overnight in lysogeny broth (LB) [62] at 37 °C, 200 rpm. 150 μL of an overnight cell suspension were spread evenly onto LB agar petri dishes. 0.15 μmol of each compound (dissolved in 10 μL or 15 μL DMSO) were applied onto circular filter paper (Ø = 6 mm, GE Healthcare). Pure DMSO, serving as a negative and CHIR-090, serving as a positive control were also spotted. The petri dishes were incubated overnight at 37 °C and the diameter of the zone of growth inhibition was measured for each compound. Each assay was performed at least three times on separate days.

4.3.2. Minimum inhibitory concentration (MIC)

The MIC values of the compounds were determined by means of the microdilution method using 96-well plates.

To determine the MIC values against *E. coli* BL21(DE3) and *E. coli* D22, the bacteria were grown overnight in LB at 37 °C and 200 rpm. The overnight suspension was diluted 1:1000 in fresh LB. 10 μL of a twofold dilution series of the compounds in DMSO and 90 μL of LB were dispensed to each well of a 96-well plate. Then, 100 μL of the inoculated medium were added, resulting in 5 · 10⁵ cfu · mL⁻¹ and a final concentration range of the test compounds between 64 μg · mL⁻¹ and 0.25 μg · mL⁻¹. The plates were incubated for 20 h at 37 °C. The MIC was defined as the lowest concentration of the compounds that prevented visible growth after incubation. Each assay was performed at least three times on separate days.

To determine the MIC values against *E. coli* C600, *E. coli* C600-R7 (Δ*tolC*), *E. coli* WT, *E. coli* WT-II (Δ*amarR175*), *E. coli* ATCC 25922, and *E. coli* ATCC 8739, the bacteria were grown overnight in LB at 37 °C and 200 rpm. The overnight suspension was diluted with sterile saline (0.9% NaCl) to yield a suspension visually equivalent to a 0.5 McFarland standard. This initial inoculum was at first diluted 1:10 with sterile saline and subsequently 1:10 with Müller-Hinton broth (MHB). 50 μL of the prepared inoculum were then dispensed to each well of a 96-well

plate. 50 μL of a two-fold dilution series of the compounds in MHB (ranging from 256 $\mu\text{g}\cdot\text{mL}^{-1}$ to 0.125 $\mu\text{g}\cdot\text{mL}^{-1}$) were finally added, resulting in final concentrations ranging from 128 $\mu\text{g}\cdot\text{mL}^{-1}$ to 0.063 $\mu\text{g}\cdot\text{mL}^{-1}$. The plates were then incubated overnight at 37 °C. The MIC was defined as the lowest concentration of the compounds that prevented visible growth after incubation.

To determine the MIC against *E. coli* ATCC 25922 and *P. aeruginosa* ATCC 27853 in the presence/absence of the efflux pump inhibitor PA β N, the bacteria were grown overnight on a LB-agar plate. The next day, one single colony was diluted with sterile saline to yield a suspension visually equivalent to a 0.5 McFarland standard. This initial inoculum was consecutively diluted 1:10 with MHB twice. 25 μL of a two-fold dilution series of the compounds in MHB (ranging from 512 $\mu\text{g}\cdot\text{mL}^{-1}$ to 1 $\mu\text{g}\cdot\text{mL}^{-1}$) were dispensed to each well of a 96-well-plate. Then, 25 μL MHB or 25 μL PA β N (256 $\mu\text{g}\cdot\text{mL}^{-1}$ in MHB) were added, respectively. Finally, 50 μL of the prepared inoculum were added, resulting in $5 \cdot 10^5$ cfu $\cdot\text{mL}^{-1}$, a final concentration range of the test compounds between 128 $\mu\text{g}\cdot\text{mL}^{-1}$ and 0.25 $\mu\text{g}\cdot\text{mL}^{-1}$, and, in case the efflux pump inhibitor was present, a PA β N concentration of 64 $\mu\text{g}\cdot\text{mL}^{-1}$. The plates were incubated for 18 h at 37 °C. The MIC was defined as the lowest concentration of the compounds that prevented visible growth after incubation.

4.4. LpxC assay

4.4.1. Protein expression

The expression of LpxCC63A was performed essentially as previously described [27]. The C63A mutation lowers the undesired influence of the Zn²⁺-concentration on the enzymatic activity.

The plasmid pETeLpxCC63A, which was kindly provided by Carol Fierke [50], was transformed into *E. coli* BL21(DE3) cells. The overnight culture was prepared by growing a single colony in 50 mL LB supplemented with carbenicillin (0.1 mM) and glucose (0.5%) at 37 °C and 200 rpm. The next day, 4 mL of this culture were used to inoculate 400 mL of fresh LB, containing carbenicillin (0.1 mM) and glucose (0.5%). After reaching an OD₆₀₀ of 0.6–0.8, the culture was cooled to 30 °C and induced with IPTG (1 mM) and ZnCl₂ (100 μM). After being grown for additional 4 h at 30 °C, the cells were cooled on ice for 20 min and then harvested by centrifugation (4 °C, 5000 g, 30 min) and stored at –20 °C.

4.4.2. Protein purification

Unless otherwise specified, all steps were carried out at 4 °C.

The harvested cells were thawed on ice and resuspended in 50 mL anion exchange (AEX)-buffer (25 mM Hepes, 2 mM DTT, pH = 6.0), containing benzamidine (15 $\mu\text{g}\cdot\text{mL}^{-1}$) and PMSF (1 mM) as protease inhibitors. Afterwards, the cells were disrupted by sonication (6 \times 20 s). Then, the cellular debris were removed by centrifugation (4 °C, 5000 g, 90 min) and the supernatant was filtered (0.2 μm).

The cleared lysate was loaded onto a 20 mL-AEX-column (HiPrep Q HP 16/10, GE Healthcare) and eluted at a flow rate of 3.0 mL $\cdot\text{min}^{-1}$ using a linear sodium chloride gradient (0 M \rightarrow 0.5 M) in AEX-buffer. The fractions containing LpxC were concentrated using molecular weight cut off (MWCO) spin columns (10 kDa), loaded onto a 120 mL-size exclusion (SEC)-column (HiLoad 16/600 Superdex 200, GE Healthcare) and eluted at a flow rate of 1.0 mL $\cdot\text{min}^{-1}$ in SEC-buffer (50 mM Bis/Tris, 150 mM NaCl, pH = 6.0). The presence of the enzyme during the purification progress was confirmed by sodium dodecyl sulphate-polyacrylamide gel electrophoresis (SDS-PAGE) with Coomassie brilliant blue staining. The purified enzyme was quantified by use of a Nanodrop 2000C, diluted with SEC-buffer to 0.5 mg $\cdot\text{mL}^{-1}$ and stored at –80 °C.

4.4.3. Enzyme inhibition assay

A fluorescence-based microplate assay for LpxC activity was performed as described by Clements et al. [17]. The wells in a black, non-binding, 96-well fluorescence microplate (Greiner Bio One,

Frickenhausen) were filled with 93 μL of 26.9 μM UDP-3-O-[(R)-3-hydroxymyristoyl]-N-acetylglucosamine in assay buffer (40 mM sodium morpholinoethanesulfonic acid, 80 μM dithiothreitol, 0.02% Brij 35 (pH 6.0)). In order to assay the inhibitors at final concentrations from 2 μM up to 200 μM , 2 μL of a respective dilution of the compounds in DMSO were added. After addition of 5 μL of a solution of purified LpxC (50 $\mu\text{g}\cdot\text{mL}^{-1}$) in assay buffer, the microplate was incubated for 30 min at 37 °C in a plate shaker. Then, the biochemical reaction was stopped by adding 40 μL of 0.625 M sodium hydroxide. The reaction mixture was further incubated for 10 min and neutralized by adding 40 μL of 0.625 M acetic acid. The deacetylated product UDP-3-O-[(R)-3-hydroxymyristoyl]glucosamine was converted into a fluorescing isoindole by adding 120 μL of a *o*-phthalaldehyde-2-mercaptoethanol solution, which was prepared by dissolving 10 mg *o*-phthalaldehyde in 1 mL methanol, diluting the mixture with 24 mL sodium borate buffer (0.1 M), and finally adding 2.5 μL 2-mercaptoethanol [63]. Fluorescence was measured with a Tristar² plate reader (Berthold, Bad Wildbad) at 340 nm excitation and 460 nm emission wavelengths. Each assay was performed at least three times on separate days. The IC₅₀ values were calculated via Probit-log concentration graphs (Figs. S3–S6) with the aid of the software Origin.

4.4.4. Quantification of 8 in subcellular compartments of *E. coli*

Compound 8 was quantified using our previously described protocol for strain cultivation, incubation, and cellular fractionation [56]. For LC/MS/MS analysis, a sample volume of 1 μL was injected. LC separations were achieved with a YMC-Pack TMS 100 mm \times 2.1 mm/S3- μm /12 nm column (YMC Europe, Dinslaken, Germany). A linear gradient using solvent A (H₂O + 0.1% formic acid) and solvent B (acetonitrile + 0.1% formic acid) was applied from 1% B to 99% B within 8.5 min at a constant flow of 0.7 mL/min. The compound eluted at a retention time of 0.69 min. A MRM (multiple reaction monitoring) method was applied, which allowed for a sensitive detection of the compound of interest. The Q1/Q3 transition masses used for compound identification are given in Table S1. The calibration curve (Fig. S2) was linear over a range of 0.4–100 ng/mL, with an $r^2 = 0.9890$. The LOD in *E. coli* whole-cell matrix was found to be 39 pg/mL.

The reported data represent the average of two biological replicates performed on different days.

4.5. Computational methods

The structures of all compounds were prepared for docking with the LigPrep module within Maestro with all settings default (Maestro version 2019-4; Schrödinger Inc, NY).

Crystal structure 3PS3 [24] was downloaded from the Protein Data Bank on March 29, 2020 and prepared with the Protein Preparation Wizard within the Maestro molecular modeling environment. As part of the preparation procedure, hydrogens were added, metals treated, and het states generated with the Epik module integrated into Maestro (all settings default). In addition, the water orientations were sampled, and the hydrogen bond network optimized (all settings default). In the final step of the protein preparation process, a restrained minimization was executed using the OPLS3e force field [64] in order to converge the heavy atoms to an RMSD of 0.30 Å (all settings default). The protonated state of His265 (HIP) that was automatically assigned by the Protein Preparation Wizard was replaced by HID in order to enable a hydrogen bond interaction with the hydroxamic acid moiety of the ligand.

Two grids were generated for docking with Glide: one including all solvent molecules and one without solvent molecules. The grid files were generated with default settings, with the location of the binding pocket defined by the position and size of the co-crystallized ligand. The hydroxyl moiety of Thr191 was defined as rotatable.

Docking was performed with the SP algorithm of GLIDE [65] with default settings. For compounds, for which no docking pose could be obtained in the presence of the solvent molecules observed in the crystal

structure that shows a chelation of the Zn^{2+} by the hydroxamic acid moiety, docking was repeated in the absence of any solvent molecules.

Declaration of Competing Interest

The authors declare that they have no known competing financial interests or personal relationships that could have appeared to influence the work reported in this paper.

Acknowledgements

This work was supported by the German Center for Infection Research (DZIF), which is gratefully acknowledged.

We thank Dr. Frank Hoffmann and Timo Stein (Institut für Anorganische und Angewandte Chemie, Universität Hamburg) for X-ray crystal structure determination and interpretation.

Appendix A. Supplementary material

Supplementary data to this article can be found online at <https://doi.org/10.1016/j.bioorg.2020.104603>.

References

- [1] R.R. Watkins, R.A. Bonomo, Overview: Global and Local Impact of Antibiotic Resistance, *Infect. Dis. Clin. North Am.* 30 (2) (2016) 313–322.
- [2] D.M. Shlaes, P.A. Bradford, Antibiotics-From There to Where?: How the antibiotic miracle is threatened by resistance and a broken market and what we can do about it, *Pathog. Immun.* 3 (1) (2018) 19–43.
- [3] H.W. Boucher, G.H. Talbot, J.S. Bradley, J.E. Edwards, D. Gilbert, L.B. Rice, M. Scheld, B. Spellberg, J. Bartlett, Bad bugs, no drugs: no ESKAPE! An update from the Infectious Diseases Society of America, *Clin. Infect. Dis.* 48 (1) (2009) 1–12.
- [4] A. Cassini, L.D. Hogberg, D. Plachouras, A. Quattrocchi, A. Hoxha, G.S. Simonsen, M. Colomb-Cotinat, M.E. Kretzschmar, B. Devleeschauwer, M. Cecchini, D. A. Ouakrim, T.C. Oliveira, M.J. Struelens, C. Suetens, D.L. Monnet, the Burden of AMR Collaborative Group, Attributable deaths and disability-adjusted life-years caused by infections with antibiotic-resistant bacteria in the EU and the European Economic Area in 2015: a population-level modelling analysis, *Lancet Infect. Dis.* 19 (1) (2019) 56–66.
- [5] E. Tacconelli, E. Carrara, A. Savoldi, S. Harbarth, M. Mendelson, D.L. Monnet, C. Pulcini, G. Kahlmeter, J. Kluytmans, Y. Carmeli, M. Ouellette, K. Outterson, J. Patel, M. Cavalieri, E.M. Cox, C.R. Houchens, M.L. Grayson, P. Hansen, N. Singh, U. Theuretzbacher, N. Magrini, WHO Pathogens Priority List Working Group, Discovery, research, and development of new antibiotics: the WHO priority list of antibiotic-resistant bacteria and tuberculosis, *Lancet Infect. Dis.* 18 (3) (2018) 318–327.
- [6] S.R. Norrby, C.E. Nord, R. Finch, Lack of development of new antimicrobial drugs: a potential serious threat to public health, *Lancet Infect. Dis.* 5 (2) (2005) 115–119.
- [7] T. Ogura, K. Inoue, T. Tatsuta, T. Suzuki, K. Karata, K. Young, L.H. Su, C.A. Fierke, J.E. Jackman, C.R.H. Raetz, J. Coleman, T. Tomoyasu, H. Matsuzawa, Balanced biosynthesis of major membrane components through regulated degradation of the committed enzyme of lipid A biosynthesis by the AAA protease FtsH (HflB) in *Escherichia coli*, *Mol. Microbiol.* 31 (3) (1999) 833–844.
- [8] M. Lakemeyer, W. Zhao, F.A. Mandl, P. Hammann, S.A. Sieber, Thinking Outside the Box-Novel Antibacterials To Tackle the Resistance Crisis, *Angew. Chem. Int. Ed. Engl.* 57 (44) (2018) 14440–14475.
- [9] M.A. Cooper, D. Shlaes, Fix the antibiotics pipeline, *Nature* 472 (7341) (2011), 32–32.
- [10] L.J. Piddock, The crisis of no new antibiotics—what is the way forward? *Lancet Infect. Dis.* 12 (3) (2012) 249–253.
- [11] S.J. Projan, P.J. Youngman, Antimicrobials: new solutions badly needed - Editorial overview, *Curr. Opin. Microbiol.* 5 (5) (2002) 463–465.
- [12] F. Narberhaus, M. Obrist, F. Fuhrer, S. Langklotz, Degradation of cytoplasmic substrates by FtsH, a membrane-anchored protease with many talents, *Res. Microbiol.* 160 (9) (2009) 652–659.
- [13] C.R.H. Raetz, C. Whitfield, Lipopolysaccharide endotoxins, *Annu. Rev. Biochem.* 71 (2002) 635–700.
- [14] C.R.H. Raetz, *Biochemistry of Endotoxins*, *Annu. Rev. Biochem.* 59 (1990) 129–170.
- [15] C.R.H. Raetz, C.M. Reynolds, M.S. Trent, R.E. Bishop, Lipid A modification systems in gram-negative bacteria, *Annu. Rev. Biochem.* 76 (2007) 295–329.
- [16] A.W. Barb, P. Zhou, Mechanism and inhibition of LpxC: an essential zinc-dependent deacetylase of bacterial lipid A synthesis, *Curr. Pharm. Biotechnol.* 9 (1) (2008) 9–15.
- [17] J.M. Clements, F. Coignard, I. Johnson, S. Chandler, S. Palan, A. Waller, J. Wijkmans, M.G. Hunter, Antibacterial activities and characterization of novel inhibitors of LpxC, *Antimicrob. Agents Chemother.* 46 (6) (2002) 1793–1799.
- [18] C.R.H. Raetz, Z.Q. Guan, B.O. Ingram, D.A. Six, F. Song, X.Y. Wang, J.S. Zhao, Discovery of new biosynthetic pathways: the lipid A story, *J. Lipid Res.* 50 (2009) S103–S108.
- [19] P.G. Sorensen, J. Lutkenhaus, K. Young, S.S. Eveland, M.S. Anderson, C.R.H. Raetz, Regulation of UDP-3-O-[R-3-hydroxymyristoyl]-N-acetylglucosamine deacetylase in *Escherichia coli* - The second enzymatic step of lipid A biosynthesis, *J. Biol. Chem.* 271 (42) (1996) 25898–25905.
- [20] G.M. Clayton, D.J. Klein, K.W. Rickert, S.B. Patel, M. Kornienko, J. Zugay-Murphy, J.C. Reid, S. Tummala, S. Sharma, S.B. Singh, L. Miesel, K.J. Lumb, S.M. Soisson, Structure of the Bacterial Deacetylase LpxC Bound to the Nucleotide Reaction Product Reveals Mechanisms of Oxyanion Stabilization and Proton Transfer, *J. Biol. Chem.* 288 (47) (2013) 34073–34080.
- [21] J.J. Robinet, J.W. Gauld, DFT investigation on the mechanism of the deacetylation reaction catalyzed by LpxC, *J. Phys. Chem. B* 112 (11) (2008) 3462–3469.
- [22] D.V. Kalinin, R. Holl, Insights into the Zinc-Dependent Deacetylase LpxC: Biochemical Properties and Inhibitor Design, *Curr. Top. Med. Chem.* 16 (21) (2016) 2379–2430.
- [23] D.V. Kalinin, R. Holl, LpxC inhibitors: a patent review (2010–2016), *Expert Opin. Ther. Pat.* 27 (11) (2017) 1227–1250.
- [24] X. Liang, C.J. Lee, X. Chen, H.S. Chung, D. Zeng, C.R. Raetz, Y. Li, P. Zhou, E. J. Toone, Syntheses, structures and antibiotic activities of LpxC inhibitors based on the diacetylene scaffold, *Bioorg. Med. Chem.* 19 (2) (2011) 852–860.
- [25] A.W. Barb, A.L. McClerren, K. Snehalatha, C.M. Reynolds, P. Zhou, C.R. Raetz, Inhibition of lipid A biosynthesis as the primary mechanism of CHIR-090 antibiotic activity in *Escherichia coli*, *Biochemistry* 46 (12) (2007) 3793–3802.
- [26] A.L. McClerren, S. Endsley, J.L. Bowman, N.H. Andersen, Z. Guan, J. Rudolph, C. R. Raetz, A slow, tight-binding inhibitor of the zinc-dependent deacetylase LpxC of lipid A biosynthesis with antibiotic activity comparable to ciprofloxacin, *Biochemistry* 44 (50) (2005) 16574–16583.
- [27] J.E. Jackman, C.A. Fierke, L.N. Tumey, M. Pirrung, T. Uchiyama, S.H. Tahir, O. Hindsgaul, C.R. Raetz, Antibacterial agents that target lipid A biosynthesis in gram-negative bacteria. Inhibition of diverse UDP-3-O-(R-3-hydroxymyristoyl)-N-acetylglucosamine deacetylases by substrate analogs containing zinc binding motifs, *J. Biol. Chem.* 275 (15) (2000) 11002–11009.
- [28] X. Li, T. Uchiyama, C.R. Raetz, O. Hindsgaul, Synthesis of a carbohydrate-derived hydroxamic acid inhibitor of the bacterial enzyme (LpxC) involved in lipid A biosynthesis, *Org. Lett.* 5 (4) (2003) 539–541.
- [29] X.C. Li, A.L. McClerren, C.R.H. Raetz, O. Hindsgaul, Mapping the active site of the bacterial enzyme LpxC using novel carbohydrate-based hydroxamic acid inhibitors, *J. Carbohydr. Chem.* 24 (4–6) (2005) 583–609.
- [30] A. Oddo, R. Holl, Design and stereoselective synthesis of a C-aryl furanoside as a conformationally constrained CHIR-090 analogue, *Carbohydr. Res.* 359 (2012) 59–64.
- [31] E. Ravarino, S.K. Jana, R. Fröhlich, R. Holl, Stereocontrolled synthesis of four diastereomeric C-aryl manno- and talofuranosides, *Carbohydr. Res.* 361 (2012) 162–169.
- [32] M. Löppenber, H. Müller, C. Pulina, A. Oddo, M. Teese, J. Jose, R. Holl, Synthesis and biological evaluation of flexible and conformationally constrained LpxC inhibitors, *Org. Biomol. Chem.* 11 (36) (2013) 6056–6070.
- [33] S.K. Jana, M. Löppenber, C.G. Daniliuc, R. Holl, Synthesis and biological evaluation of C-ethynyl furanosides as LpxC inhibitors, *Tetrahedron* 71 (6) (2015) 956–966.
- [34] S.K. Jana, M. Löppenber, C.G. Daniliuc, R. Holl, C-Triazolyl beta-D-furanosides as LpxC inhibitors: stereoselective synthesis and biological evaluation, *Tetrahedron* 70 (37) (2014) 6569–6577.
- [35] S.K. Jana, M. Löppenber, C.G. Daniliuc, J. Jose, R. Holl, Development of novel LpxC inhibitors: chiral-pool synthesis of C-triazolyl glycosides, *Tetrahedron* 69 (45) (2013) 9434–9442.
- [36] H. Müller, V. Gabrielli, O. Agoglitto, R. Holl, Chiral pool synthesis and biological evaluation of C-furanosidic and acyclic LpxC inhibitors, *Eur. J. Med. Chem.* 110 (2016) 340–375.
- [37] A. Dreger, O. Kharwb, O. Agoglitto, E.F. Bülbül, J. Melesina, W. Sippl, R. Holl, Chiral Pool Synthesis, Biological Evaluation and Molecular Docking Studies of C-Furanosidic LpxC Inhibitors, *ChemMedChem* 14 (8) (2019) 871–886.
- [38] S.F. Jenkinson, T. Harris, G.W.J. Fleet, Oxetane cis- and trans beta-amino-acid scaffolds from D-xylose by efficient S(N)2 reactions in oxetane rings: methyl and hydroxymethyl analogues of the antibiotic oxetin, an oxetane beta-amino-acid, *Tetrahedron-Asymmetr.* 15 (17) (2004) 2667–2679.
- [39] S.D. Lucas, A.P. Rauter, J. Schneider, H.P. Wessel, Synthesis of 3-Fluoro-Oxetane delta-Amino Acids, *J. Carbohydr. Chem.* 28 (7–8) (2009) 431–446.
- [40] H. Zhang, P.F. Liu, Q. Chen, Q.Y. Wu, A. Seville, Y.C. Gu, J. Clough, S.L. Zhou, G. F. Yang, Synthesis and absolute configuration assignment of albiducin: a late-stage reductive deiodination by visible light photocatalysis, *Org. Biomol. Chem.* 14 (13) (2016) 3482–3485.
- [41] T.K.M. Shing, J.G. Gillhouley, Enantiospecific Synthesis of (+)-Altholactone and Its 3 Stereoisomers, *Tetrahedron* 50 (29) (1994) 8685–8698.
- [42] J. Einhorn, C. Einhorn, F. Ratajczak, J.L. Pierre, Efficient and Highly Selective Oxidation of Primary Alcohols to Aldehydes by N-Chlorosuccinimide Mediated by Oxoammonium Salts, *J. Org. Chem.* 61 (21) (1996) 7452–7454.
- [43] S. Front, S. Almeida, V. Zoete, J. Charollais-Thoening, E. Gallienne, C. Marmy, V. Pilloud, R. Marti, T. Wood, O.R. Martin, S. Demotz, 4-epi-Isogomine derivatives as pharmacological chaperones for the treatment of lysosomal diseases linked to beta-galactosidase mutations: Improved synthesis and biological investigations, *Bioorg. Med. Chem.* 26 (20) (2018) 5462–5469.

- [44] M. Jeselnik, I. Leban, S. Polanc, M. Kocevar, D-Gulonolactone as a synthon for L-noviose: first preparation of 4-O-demethyl-L-noviofuranose and related derivatives, *Org. Lett.* 5 (15) (2003) 2651–2653.
- [45] R.E. Ireland, P. Maienfisch, The convergent synthesis of polyether ionophore antibiotics: the synthesis of the A ring carbamonensin spiro ether, *J. Organ. Chem.* 53 (3) (1988) 640–651.
- [46] D. Cremer, J.A. Pople, General definition of ring puckering coordinates, *J. Am. Chem. Soc.* 97 (6) (1975) 1354–1358.
- [47] S. Normark, H.G. Boman, E. Matsson, Mutant of *Escherichia coli* with Anomalous Cell Division and Ability to Decrease Episomally and Chromosomally Mediated Resistance to Ampicillin and Several Other Antibiotics, *J. Bacteriol.* 97 (3) (1969) 1334–1342.
- [48] T. Grundstrom, S. Normark, K.E. Magnusson, Overproduction of Outer-Membrane Protein Suppresses EnvA-Induced Hyperpermeability, *J. Bacteriol.* 144 (3) (1980) 884–890.
- [49] B. Beall, J. Lutkenhaus, Sequence-Analysis, Transcriptional Organization, and Insertional Mutagenesis of the *EnvA* Gene of *Escherichia-Coli*, *J. Bacteriol.* 169 (12) (1987) 5408–5415.
- [50] M. Hernick, S.G. Gattis, J.E. Penner-Hahn, C.A. Fierke, Activation of *Escherichia coli* UDP-3-O-[(R)-3-hydroxymyristoyl]-N-acetylglucosamine Deacetylase by Fe^{2+} Yields a More Efficient Enzyme with Altered Ligand Affinity, *Biochemistry* 49 (10) (2010) 2246–2255.
- [51] J.E. Jackman, C.R. Raetz, C.A. Fierke, UDP-3-O-(R-3-hydroxymyristoyl)-N-acetylglucosamine deacetylase of *Escherichia coli* is a zinc metalloenzyme, *Biochemistry* 38 (6) (1999) 1902–1911.
- [52] C. Yilmaz, G. Ozcengiz, Antibiotics: Pharmacokinetics, toxicity, resistance and multidrug efflux pumps, *Biochem. Pharmacol.* 133 (2017) 43–62.
- [53] J.M. Blair, M.A. Webber, A.J. Baylay, D.O. Ogbolu, L.J. Piddock, Molecular mechanisms of antibiotic resistance, *Nat. Rev. Microbiol.* 13 (1) (2015) 42–51.
- [54] P. Heisig, R. Tschorny, Characterization of fluoroquinolone-resistant mutants of *escherichia coli* selected in vitro, *Antimicrob. Agents Chemother.* 38 (6) (1994) 1284–1291.
- [55] A. Schulte, P. Heisig, In vitro activity of gemifloxacin and five other fluoroquinolones against defined isogenic mutants of *Escherichia coli*, *Pseudomonas aeruginosa* and *Staphylococcus aureus*, *J. Antimicrob. Chemother.* 46 (6) (2000) 1037–1038.
- [56] H. Prochnow, V. Fetz, S.K. Hotop, M.A. Garcia-Rivera, A. Heumann, M. Brönstrup, Subcellular Quantification of Uptake in Gram-Negative Bacteria, *Anal. Chem.* 91 (3) (2019) 1863–1872.
- [57] R.H. Blessing, An empirical correction for absorption anisotropy, *Acta Crystallogr. A* 51 (Pt 1) (1995) 33–38.
- [58] W.R. Busing, H.A. Levy, High-speed computation of the absorption correction for single-crystal diffraction measurements, *Acta Crystallogr. A* 10 (3) (1957) 180–182.
- [59] O.V. Dolomanov, L.J. Bourhis, R.J. Gildea, J.A.K. Howard, H. Puschmann, OLEX2: a complete structure solution, refinement and analysis program, *J. Appl. Crystallogr.* 42 (2) (2009) 339–341.
- [60] G. Sheldrick, SHELXT - Integrated space-group and crystal-structure determination, *Acta Crystallogr. Sect. A* 71 (1) (2015) 3–8.
- [61] A. Spek, Structure validation in chemical crystallography, *Acta Crystallogr. Sect. D* 65 (2) (2009) 148–155.
- [62] G. Bertani, Studies on lysogenesis. I. The mode of phage liberation by lysogenic *Escherichia coli*, *J. Bacteriol.* 62 (3) (1951) 293–300.
- [63] M. Roth, Fluorescence Reaction for Amino Acids, *Anal. Chem.* 43 (7) (1971) 880–882.
- [64] K. Roos, C. Wu, W. Damm, M. Reboul, J.M. Stevenson, C. Lu, M.K. Dahlgren, S. Mondal, W. Chen, L. Wang, R. Abel, R.A. Friesner, E.D. Harder, OPLS3e: Extending Force Field Coverage for Drug-Like Small Molecules, *J. Chem. Theory Comput.* 15 (3) (2019) 1863–1874.
- [65] R.A. Friesner, J.L. Banks, R.B. Murphy, T.A. Halgren, J.J. Klicic, D.T. Mainz, M. P. Repasky, E.H. Knoll, M. Shelley, J.K. Perry, D.E. Shaw, P. Francis, P.S. Shenkin, Glide: a new approach for rapid, accurate docking and scoring. 1. Method and assessment of docking accuracy, *J. Med. Chem.* 47 (7) (2004) 1739–1749.